

## Determination of the linear elastic stiffness and hygroexpansion of softwood by a multilayered unit cell using poromechanics

Stefan Gloimüller\*, Karin de Borst, Thomas K. Bader and Josef Eberhardsteiner

*Institute for Mechanics of Materials and Structures, Vienna University of Technology,  
Karlsplatz 13/202, A-1040 Vienna, Austria*

*(Received August 17, 2011, Revised May 23, 2012, Accepted August 27, 2012)*

**Abstract.** Hygroexpansion of wood is a known and undesired characteristic in civil engineering. When wood is exposed to changing environmental humidity, it adsorbs or desorbs moisture and warps. The resulting distortions or - at restrained conditions - cracks are a major concern in timber engineering. We herein present a multiscale model for prediction of the macroscopic hygroexpansion behavior of individual pieces of softwood from their microstructure, demonstrated for spruce. By applying poromicromechanics, we establish a link between the swelling pressure, driving the hygroexpansion of wood at the nanoscale, and the resulting macroscopic dimensional changes. The model comprises six homogenization steps, which are performed by means of continuum micromechanics, the unit cell method and laminate theory, all formulated in a poromechanical framework. Model predictions for elastic properties of wood as functions of the moisture content closely approach corresponding experimental data. As for the hygroexpansion behavior, the swelling pressure has to be back-calculated from macroscopic hygroexpansion data. The good reproduction of the anisotropy of wood hygroexpansion, based on only a single scalar calibration parameter, underlines the suitability of the model. The multiscale model constitutes a valuable tool for studying the effect of microstructural features on the macroscopic behavior and for assessing the hygroexpansion behavior at smaller length scales, which are inaccessible to experiments. The model predictions deliver input parameters for the analysis of timber at the structural scale, therewith enabling to optimize the use of timber and to prevent moisture-induced damage or failure.

**Keywords:** wood; hygroexpansion; multilayered unit cell; microstructure; anisotropy; poromechanics; ray cells; earlywood; latewood.

---

### 1. Introduction

Wood is a hygroscopic material - it can adsorb or desorb moisture from the atmosphere and, therewith, adjust its moisture content to the relative humidity of the surrounding. This characteristic of wood is one of the main concerns in timber engineering. If the swelling or shrinkage upon changes of the moisture content is constrained, considerable stresses may build up and cause cracking of the material at macroscopic and microscopic levels. Especially at rapidly and often changing indoor

---

\* Corresponding author, Research Assistant, E-mail: [stefan.gloimueller@bfk-krems.at](mailto:stefan.gloimueller@bfk-krems.at)

humidity the crack risk is high. Moreover great pressures of time in construction progress often lead to insufficient wood drying. Continuing drying of mounted timber members to a moisture content (MC) in equilibrium with the surrounding air humidity results in restraints in statically indeterminate constructions and possibly in building defects. Different shrinkage behaviors of wood in its principal material directions (radial -  $R$  [normal to the plane of the annual ring layers], tangential -  $T$  [transversal direction along the annual rings], and longitudinal -  $L$  [grain direction]), may also cause deformations like bow, cup and crook. Such deformations might entirely spoil the material and, thus, have a considerable economic impact. The hygroexpansion of wood is influenced by effects acting at different length scales from micro- to macroscopic level. The microstructural origin of drying anisotropy motivates the development of multiscale models herein in order to describe the macroscopic drying behavior of wood. Starting at sufficiently low length scales, i.e., at a level below the cell wall where water is released from the cell wall material upon drying, and applying a poromechanical approach allows emanating from physical principles and linking fundamental properties to macroscopic characteristics by means of homogenization schemes. This way, universally applicable and predictive models are obtained. The microstructural assembly of softwood is replicated first, followed by a short review of the current state of the art in modeling of the hygroexpansion behavior of wood. Homogenization methods used in this model are reviewed in a theoretical manner and applied to softwood in a following section. Existing multiscale models for wood are extended by consideration of the individual cell wall layers, of the annual rings composed of earlywood and latewood, and of ray cells in order to suitably capture all microstructural effects on the hygroexpansion behavior. The corresponding additional physical and chemical properties of softwood, serving as input parameters for the homogenization steps, are discussed as well. This is followed by poromechanical values of softwood as output of the homogenization procedure. Swelling pressure and therefrom resulting hygroexpansion coefficients are focused on in the last section, followed by conclusions.

## **2. Background**

### *2.1 Microstructural assembly of softwood*

The macroscopic hygromechanical behavior of wood is a consequence of the superposition of different deformation mechanism at various length scales. In order to understand the influences evolving from the different scales, the hierarchical structure of wood is shortly reviewed first, specifying also required input parameters for the multiscale model.

#### *2.1.1 Nano and micro scales*

At the nanoscale the principal components of wood are crystalline cellulose, extractives, lignin, amorphous cellulose and hemicelluloses, listed according to their sorption capacity, starting with the most hydrophobic constituent. Cellulose is assembled into microfibrils with a core of hydrophobic crystalline cellulose surrounded by an hydrophilic amorphous part with a volumetric content of approximately 1/3 of cellulose. The microfibrils show different inclinations to the longitudinal axis (microfibril angle -MFA) in each cell wall layer, see Table 1, and are surrounded by a matrix made up of lignin and hemicelluloses connecting the fibrils. At moist conditions, water molecules interpenetrate the matrix and are bound either chemically at low moisture contents (0% to ~ 6% MC, 'chemisorption') or physically (~ 6% to ~ 15% MC, 'physisorption', ~ 15% to fiber saturation

Table 1 Morphological and chemical cell wall layer characteristics typical for spruce, used in the model shown in Section 3, (Fengel and Wegener 1983, Qing and Mishnaevsky 2008, Fratzl and Weinkamer 2007, Neagu and Gamstedt 2007)

		Earlywood / latewood					
		<i>ML</i>	<i>P</i>	<i>S1</i>	<i>S2</i>	<i>S3</i>	<i>CW</i>
Cell wall layer thickness	[ $\mu\text{m}$ ]	0.25	0.10	0.20/0.30	1.42/4.48	0.03/0.04	3.96/9.38
Microfibril angle	[deg]		45	50	10/5	75	
Microfibril winding orientation	[helix]		<i>Z</i>	<i>X</i>	<i>S</i>	<i>Z</i>	
Weight fraction cellulose		0.119	0.147	0.262	0.522	0.475	
Weight fraction hemicelluloses		0.319	0.300	0.299	0.262	0.359	
Weight fraction lignin		0.531	0.522	0.408	0.185	0.135	
Weight fraction extractives				0.031			

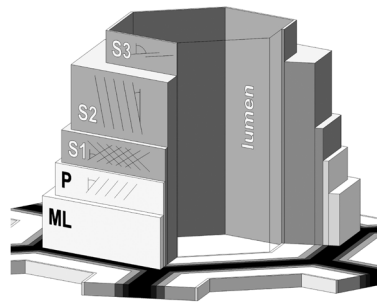


Fig. 1 Model of the layered softwood cell

point, ‘capillary condensation’), to the wood polymers. This storage process of water in the cell wall causes the swelling of wood known as hygroexpansion and leads also to maceration and prestressing of the cell wall material. Due to the ellipsoidal shape of the stiff and mainly hydrophobic microfibrils, expansion develops preferably in transversal direction and is heavily restrained in the longitudinal direction of the fibrils.

### 2.1.2 Meso scale - cell wall layers

In softwood, cell walls of earlywood and latewood consist of five cell wall layers with different chemical compositions, microfibril angles and microfibril winding orientations (cf. also Table 1 and Fig. 1).

The *middle lamella* - *ML* - is nearly free of cellulose, but undergoes a relatively high isotropic expansion upon moistening due to the high concentration of hemicellulose. The *primary cell wall* - *P* - is a thin layer, which is formed during cell growth by attaching cellulose microfibrils with a high and right-turning inclination angle to the middle lamella. In the *first layer of the secondary wall* - *S1*, a high microfibril angle of the crosswisely arranged fibrils (denoted by *X*-helix) results in high stiffness in the longitudinal direction and a transverse restraining of hygroexpansion. The *second layer* of the secondary wall - *S2* - is responsible for the variable cell wall thicknesses in early- and latewood and accounts for 80-90% of the cell wall volume (Kollmann 1951, Astley *et al.* 1998, Persson 2000, Bergander 2001). With its small and left-turning winding microfibril angle and

Table 2 Characteristics of earlywood and latewood (Fengel and Wegener 1983, Kollmann 1951),  $\ell_R$  and  $\ell_T$  refer to the radial and tangential dimension of a wood cell,  $\varphi$  to the inclination angle of the radial cell wall against the radial axis, and  $\beta$  to the cell wall opening angle, as used in the model ( $\rho_{wet}$  specified for  $MC = 12\%$ )

	Cell diameters		$\rho_{wet}$	$\varphi$	$\beta$
	$\ell_R$	$\ell_T$			
	[ $\mu m$ ]	[ $\mu m$ ]			
Earlywood	35	30	~0.36	21	2
Latewood	28	30	~0.88	5	1
Ray cells	40	30	~0.33	13	0

the high cellulose content, it is the main supporting element in longitudinal direction. The maximum hygroexpansion in transverse direction is again reduced by *the third layer of the secondary wall - S3* - due to its very high, right-turning microfibril angle. The unconstrained main swelling direction is for all layers orthogonal to the axial direction of the cellulose microfibrils.

### 2.1.3 Meso scale - wood cells

Wood cells are hollow tubes oriented in the longitudinal direction with a nearly quadratic or hexagonal cross-section, different diameters in radial and tangential direction, and varying cell wall thicknesses between earlywood and latewood (see Table 2).

### 2.1.4 Macro scale - ray cell bundles

Ray cell bundles running in *R*-direction reinforce the layered wood structure in this direction. The cross-section of a ray cell bundle consists of multiple tracheids with a nearly circular cross-section, arranged in columns (single-row in coniferous wood, multi-row in hardwood) in *L*-direction. As a first assumption and in view of the similar densities, the chemical composition of the ray cell wall layers is set equal to that of the longitudinally oriented cells (tracheids). Also the microfibril angles and winding directions in each cell wall layer correspond to that of earlywood except for a higher MFA of the *S2*-layer of  $\theta_{ray,S2} = 40^\circ$  (Burgert 2000). This leads to a lower stiffness in axial direction. In spruce wood the volume fraction of ray cell bundles ranges from 1 to 10% (Fengel and Wegener 1983, Boutelje 1962, Burgert 2003, Kollmann 1951, Olsson *et al.* 2001, Tarmian and Azadfallah 2009). Besides their restraining effect in radial direction, they slightly reduce stiffness in tangential and also in longitudinal direction.

## 2.2 State-of-the-art of wood hygroexpansion and its homogenization

Examination of the microstructural origin of the anisotropic shrinkage behavior of wood has already attracted considerable scientific attention. For example Pang and Herritsch (2005) investigated experimentally the anisotropic shrinkage of pine earlywood and latewood, and Perré and Huber (2007) measured the moisture induced expansion of spruce earlywood and latewood at the tissue level on slitted samples using an optical measurement method.

As regards modeling, Kifetew (1997) and Kifetew *et al.* (1997) investigated the reasons for shrinkage anisotropy of Scots pine considering the earlywood-latewood interaction. Yamamoto (1999) developed a model of the anisotropic shrinking process of wood. Considering a single fiber

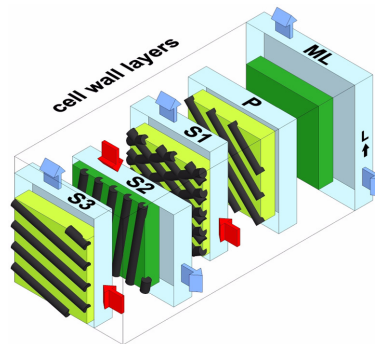


Fig. 2 Microfibril angles and their effects on swelling - enclosing open cuboids at each cell wall layer show the deformed shape without cell wall layer interaction, red arrows mark the restraining effects of the microfibrils, and blue arrows indicate the main swelling direction

with different properties of the cell wall layers was also done with more sophisticated geometric models by Qing and Mishnaevsky Jr (2009). Pang (2002) formulated a model to predict the shrinkage of wood cells from the shrinkage of the wood cell wall, from changes in lumen shape, and from effects of rays and bordered pits. Nakano (2008) examined the relationship between inward and outward swelling of cell wall surfaces, based on a cylindrical model of wood cells. Marklund and Varna (2009) analyzed the hygroexpansion of the wood fiber composite concerning the effect of wood fiber ultrastructure and cell wall hygroelastic properties. All these models are restricted to certain microstructural features and effects. Herein, we strive for a representation of the entire hierarchical structure of wood and for resolving the origin of hygroexpansion as swelling pressure on the scale of the cell wall matrix. Particular emphasis is laid on the behavior of the wood cell structure as a honeycomb of multi-layered hexagonal cylinders. A poromechanical formulation of the unit cell method is applied in order to link stiffness properties and swelling pressures of the individual cell wall layers to corresponding quantities of earlywood or latewood. With the model we intend to study (1) the interaction between earlywood and latewood, (2) the restraining effect of ray cells, (3) different swelling behavior of the cell wall layers, (4) different inclination angles of the microfibrils in radial and tangential walls and (5) different cell wall thicknesses as effects for the drying anisotropy mentioned before. The micromechanical model described in the following provides a mathematical description of these relations.

### 2.3 Fundamentals of poromicromechanics

We apply poromechanics to develop a multiscale model for the hygroexpansion behavior of wood. Depending on the particular microstructure observed at the various length scales, different homogenization techniques are employed: continuum micromechanics for a random microstructure, the unit cell method for a periodic microstructure, and laminate theory for a layered microstructure. These methods and their poromechanical extensions are briefly reviewed next. Continuum micromechanics.

In continuum micromechanics, the heterogeneous random microstructure of a material is resolved within a so-called representative volume element (RVE) composed of homogenized subdomains, so called phases. The elastic behavior of the homogenized material is determined from stiffnesses and

dosages of phases in the RVE, for characteristic shapes of the inclusions making up the phases and interactions between the phases. Zaoui (2002) formulated the relation between estimates for the homogenized stiffness tensor of a material,  $\mathbb{C}^{hom}$ , and the stiffness matrices  $\mathbb{C}_r$  and volume fractions  $f_r$  of the phases in the following most general form as

$$\mathbb{C}^{hom} = \langle \mathbb{C}_r : \mathbb{A}_r \rangle = \sum_r f_r \mathbb{C}_r : \mathbb{A}_r, \quad (1)$$

where the strain concentration tensors  $\mathbb{A}_r$  read as

$$\mathbb{A}_r = [\mathbb{I} + \mathbb{P}_r^0 : (\mathbb{C}_r - \mathbb{C}^0)]^{-1} : \left\{ \sum_s f_s [\mathbb{I} + \mathbb{P}_s^0 : (\mathbb{C}_s - \mathbb{C}^0)]^{-1} \right\}^{-1}. \quad (2)$$

Therein,  $\mathbb{P}_r^0$  refers to the Hill tensor of phase  $r$ , depending on the inclusion shape and the stiffness of the embedding medium.  $\mathbb{I}$  stands for the fourth-order symmetric unity tensor. The two sums in Eqs. (1) and (2) are taken over all phases in the RVE.  $\mathbb{C}^0$  is the fourth-order stiffness tensor of the reference medium. For the case of a particle-reinforced composite,  $\mathbb{C}^0$  is generally chosen as the stiffness of the continuous matrix material, resulting in a Mori-Tanaka model with  $\mathbb{C}_{MT}^{hom}$  as resulting homogenized stiffness tensor. In the self-consistent scheme,  $\mathbb{C}^0$  equals  $\mathbb{C}_{SC}^{hom}$ , with  $\mathbb{C}_{SC}^{hom}$  being the sought homogenized stiffness itself. This requires an iterative solution method for calculating  $\mathbb{C}_{SC}^{hom}$  (Zaoui 2002). Since there is no matrix in the self-consistent scheme, the constituents show high volume fraction, except those with no stiffness like water or air (pores). Here the calculations end up with volume fractions of 49%.

### 2.3.1 Continuum poromechanics

A poroelastic material is considered to consist of a solid matrix  $s$  and the pore space  $p$ . The pore space is characterized by stiffness  $\mathbb{C}_p = 0$  and a volume fraction equal to the porosity  $f_p = \phi_0$ . If the pore space is saturated, but no pressure is exerted onto the fluid, so that it can freely enter and leave the pore space ( $p = 0$ ), conditions are called drained. Stresses arising from a non-zero pressure  $\mathbf{p} = p \mathbf{1}$  can be considered as eigenstress  $\sigma_p^T = -p \mathbf{1}$ . Following Biot (1955), Dormieux *et al.* (2002) and Hellmich and Ulm (2005), the upscaling of eigenstresses  $\sigma_r^T$  and of eigenstrains  $\varepsilon_r^T$  in the phases to corresponding macroscopic quantities  $\Sigma^T$  and  $\mathbf{E}^T$ , respectively, is achieved using the strain concentration tensors  $\mathbb{A}_r$  and the stress concentration tensors  $\mathbb{B}_r$ ,

$$\Sigma^T = \langle \sigma^T : \mathbb{A} \rangle = \sum_r f_r \sigma_r^T : \mathbb{A}_r \quad \text{and} \quad \mathbf{E}^T = \langle \varepsilon^T : \mathbb{B} \rangle = \sum_r f_r \varepsilon_r^T : \mathbb{B}_r. \quad (3)$$

Thus, the macroscopic eigenstress resulting from pore pressure  $p$  reads as

$$\Sigma^T = -\phi_0 p \mathbf{1} : \mathbb{A}_p. \quad (4)$$

Inserting Eq. (4) into the general relation

$$\Sigma = \mathbb{C}^{hom} : \mathbf{E} + \Sigma^T, \quad (5)$$

and considering the homogenized (effective) stiffness of the material with empty pores

$$\mathbb{C}^{hom,empty} = (1 - \phi_0) \mathbb{C}_s : \mathbb{A}_s = \mathbb{C}^{hom,drained}, \quad (6)$$

yields the first poromechanical state equation

$$\Sigma + \mathbf{b}^{hom} p = \mathbb{C}^{hom,empty} : \mathbf{E} \quad \text{with} \quad \mathbf{b}^{hom} = \phi_0 \mathbf{1} : \mathbb{A}_p. \quad (7)$$

Therein, the homogenized (effective) Biot tensor  $\mathbf{b}^{hom}$  ( $b_{ij} < 1$ ) describes the macroscopic stress resulting from pore pressure  $p$  at restrained boundary conditions  $\mathbf{E} = 0$ .  $\mathbb{C}_s$  and  $\mathbb{A}_s$  denote stiffness tensor and strain concentration tensor of the solid matrix. The change of porosity

$$\phi - \phi_0 = \phi_0 \mathbf{1} : \varepsilon_p, \quad (8)$$

results from the combined action of pore pressure  $p$  and macroscopic strain  $\mathbf{E}$  and reads as (Hellmich and Ulm 2005)

$$(\phi - \phi_0) = \mathbf{b}^{hom} : \mathbf{E} + \frac{p}{N^{hom}}. \quad (9)$$

This is the second state equation of poroelasticity, which is formulated in terms of the inverse of the Biot modulus  $N^{hom}$  for the effective homogeneous material

$$\frac{1}{N^{hom}} = \mathbf{1} : \mathbb{C}_s^{-1} : (\mathbf{b}^{hom} - \phi_0 \mathbf{1}). \quad (10)$$

If the porous material is sealed at its boundary (undrained conditions), the requirement of constant fluid mass in the RVE,  $m = const. \rightarrow dm = 0$ , allows to relate the pore pressure to the macroscopic strain  $\mathbf{E}$ . Using a linear constitutive law for the fluid with bulk modulus  $k_f$ , this relation reads as (Hellmich and Ulm 2005)

$$p = -\left(\frac{\phi_0}{k_f} + \frac{1}{N^{hom}}\right)^{-1} \mathbf{b}^{hom} : \mathbf{E}. \quad (11)$$

Finally, inserting Eq. (11) in the first state equation (Eq. (7))

$$\Sigma = \mathbb{C}^{hom,drained} : \mathbf{E} + \mathbf{b}^{hom} \otimes \left(\frac{\phi_0}{k_f} + \frac{1}{N^{hom}}\right)^{-1} \mathbf{b}^{hom} : \mathbf{E} = \mathbb{C}^{hom,undrained} : \mathbf{E}, \quad (12)$$

yields the stiffness tensors at undrained conditions

$$\mathbb{C}^{hom,undrained} = \mathbb{C}^{hom,drained} + M \mathbf{b}^{hom} \otimes \mathbf{b}^{hom}, \quad (13)$$

with the so-called effective Biot modulus of the porous continuum or overall Biot modulus

$$\frac{1}{M^{hom}} = \frac{\phi_0}{k_f} + \frac{1}{N^{hom}}. \quad (14)$$

### 2.3.2 Unit cell method

In the unit cell method, the heterogeneous microstructure is represented by the basic periodically repeating unit (unit cell). The homogenized stiffness is determined from the relation between

macroscopic strains applied to the unit cell and the resulting macroscopic stresses which are volume averages over the microstresses in the unit cell. In order to identify these relations, six independent displacement configurations are imposed onto the boundary of the unit cell, corresponding to a unit value of one particular macroscopic strain component  $E_{ij, i,j} = 1, 2, 3$  at a time and zero macroscopic strain components otherwise (Hofstetter *et al.* 2006). In addition, periodic and - in case of exploiting symmetry of the unit cell and its loading state - possibly also symmetric or antisymmetric boundary conditions are applied for the displacements (Böhm 2004). The components of the homogenized stiffness tensor  $\mathbb{C}_{UC}^{hom}$  are equal to the volume averages of the corresponding periodic microstresses column by column.

### 2.3.3 Unit cell-based poromechanical homogenization techniques

In a poromechanical framework, the mentioned six reference strain states, evaluated at zero pore pressure, yield the components of the drained homogenized stiffness tensor. An additional loading case  $\mathbf{E} = 0$  and  $p = 1$ , applying a unit pore pressure in a deformation-restrained unit cell, allows to directly derive the poroelastic constants. From the first state equation of poromechanics (cf. Eq. (7)), the components of the homogenized Biot tensor are obtained as the spatial averages of macroscopic stresses

$$\Sigma = \mathbb{C}^{hom, drained} : \underbrace{\mathbf{E}}_{=0} - \mathbf{b}^{hom} \underbrace{p}_{=1} \Rightarrow \mathbf{b}^{hom} = -\Sigma. \quad (15)$$

Evaluating, for the same loading conditions, the change of porosity gives direct access to the homogenized Biot modulus  $N^{hom}$  from the second state equation (cf. Eq. (9))

$$(\phi - \phi_0) = \mathbf{b}^{hom} : \underbrace{\mathbf{E}}_{=0} + \underbrace{p}_{=1} \frac{1}{N^{hom}} \Rightarrow N^{hom} = \frac{1}{(\phi - \phi_0)}. \quad (16)$$

With these poromechanical material characteristics  $\mathbf{b}^{hom}$  and  $N^{hom}$ , the stiffness tensor at undrained conditions and the overall Biot modulus  $M^{hom}$  can be calculated following Eqs. (13) and (14).

### 2.3.4 Poromechanical laminate theory

For a layered structure, effective poromechanical properties are derived by means of a three-dimensional formulation of laminate theory presented by El Omri *et al.* (2000) and Ulm *et al.* (2004). For an array with homogeneous layers perpendicular to coordinate axis  $\mathbf{e}_1$ , the inherent assumption in laminate theory is that the strain components  $\varepsilon_{22}$ ,  $\varepsilon_{33}$  and  $\varepsilon_{23}$  as well as the stress components  $\sigma_{11}$ ,  $\sigma_{12}$  and  $\sigma_{31}$  are uniform for all layers. The derivation of the drained stiffness tensor  $\mathbb{C}^{hom, drained}$  and the poromechanical characteristics  $\mathbf{b}^{hom}$  and  $N^{hom}$  of a multilayered material is based on a separation of plane and antiplane contributions to the poroelastic state equation

$$\begin{bmatrix} \boldsymbol{\sigma}_p \\ \boldsymbol{\sigma}_a \end{bmatrix} = \begin{bmatrix} \mathbb{C}_{pp} & \mathbb{C}_{pa} \\ \mathbb{C}_{pa} & \mathbb{C}_{aa} \end{bmatrix} \begin{bmatrix} \boldsymbol{\varepsilon}_p \\ \boldsymbol{\varepsilon}_a \end{bmatrix} - \begin{bmatrix} \mathbf{b}_p \\ \mathbf{b}_a \end{bmatrix} p, \quad (17)$$

with  $p$  referring to the plane components 11, 12 and 22, and  $a$  to the antiplane components 33, 31 and 32. A matrix operator  $S$  is introduced to sort the tensor components into plane, planeantiplane,

antiplane-plane and antiplane parts (cf. (Ulm *et al.* 2004), where this operator is denoted with  $\mathbb{P}$ ). Taking the drained stiffness tensor of one layer as example, this split reads as

$$\mathbb{C}_{layer}^{drained,sorted} = \mathbf{S}^T \cdot \mathbb{C}_{layer}^{drained} \cdot \mathbf{S} = \begin{bmatrix} \mathbb{C}_{pp} & \mathbb{C}_{pa} \\ \mathbb{C}_{ap} & \mathbb{C}_{aa} \end{bmatrix}_{layer}^{drained,sorted}. \quad (18)$$

Considering  $\varepsilon_p = E_p$  and  $\sigma_A = \Sigma_A$ , the first (elastic) part of Eq. (17) can be written as

$$\begin{bmatrix} \sigma_p \\ \varepsilon_a \end{bmatrix} = \begin{bmatrix} \mathbb{K}_{pp} & \mathbb{K}_{pa} \\ \mathbb{K}_{ap} & \mathbb{K}_{aa} \end{bmatrix} \begin{bmatrix} \mathbf{E}_p \\ \Sigma_a \end{bmatrix}, \quad (19)$$

where the involved plane ( $p$ ) and antiplane ( $a$ ) parts of the fourth-order stiffness tensor components of one lamella follow from

$$\begin{aligned} \mathbb{K}_{pp} &= \mathbb{C}_{pp} - \mathbb{C}_{pa} : \mathbb{C}_{aa}^{-1} : \mathbb{C}_{ap}, & \mathbb{K}_{pa} &= \mathbb{C}_{pa} : \mathbb{C}_{aa}^{-1} \\ \mathbb{K}_{ap} &= -\mathbb{C}_{aa}^{-1} : \mathbb{C}_{ap}, & \mathbb{K}_{aa} &= \mathbb{C}_{aa}^{-1} \end{aligned}. \quad (20)$$

Volume averaging over all layers yields

$$\mathbb{K}_{ij} = \sum_{layer} f_{layer} \mathbb{K}_{ij} \quad i, j \in \{a, p\}, \quad (21)$$

where  $f_{layer}$  denotes the volume fraction (=relative thickness) of a specific layer. Finally, partial inversion of Eq. (19) results in the effective stiffness of the layered composite as

$$\begin{aligned} \mathbb{C}_{pp} &= \mathbb{K}_{pp} - \mathbb{K}_{pa} : \mathbb{K}_{aa}^{-1} : \mathbb{K}_{ap}, & \mathbb{C}_{pa} &= \mathbb{K}_{pa} : \mathbb{K}_{aa}^{-1} \\ \mathbb{C}_{ap} &= \mathbb{C}_{pa}, & \mathbb{C}_{aa} &= \mathbb{K}_{aa}^{-1} \end{aligned}, \quad (22)$$

and, after rearranging, as

$$\mathbb{C}^{hom,drained} = \mathbf{S} \cdot \begin{bmatrix} \mathbb{C}_{pp} & \mathbb{C}_{pa} \\ \mathbb{C}_{ap} & \mathbb{C}_{aa} \end{bmatrix}^{drained,sorted} \cdot \mathbf{S}^T. \quad (23)$$

The same procedure is applied to the poromechanical part of Eq. (17). Separation of the plane and antiplane parts of the Biot tensors

$$\beta_{layer} = \mathbf{S}^T \cdot \mathbf{b}_{layer} = \begin{bmatrix} \beta_p \\ \beta_a \end{bmatrix}_{layer}, \quad (24)$$

and partial inversion of the constitutive law of one lamella leads to

$$\begin{aligned} \mathbf{l}_p &= \beta_p - \mathbb{C}_{pa} : \mathbb{C}_{aa}^{-1} : \beta_a \\ \mathbf{l}_a &= -\mathbb{C}_{aa}^{-1} : \beta_a \end{aligned}. \quad (25)$$

Volume averaging over all layers yields

$$\mathbf{L}_i = \sum_{layer} f_{layer} \mathbf{l}_i \quad i \in \{a, p\}. \quad (26)$$

Finally, the effective Biot tensor of the layered composition is estimated by partial inversion of

Eq. (19), reading as

$$\begin{aligned}\mathbf{B}_p &= \mathbf{L}p - \mathbb{K}_{pa} : \mathbb{K}_{aa}^{-1} : \mathbf{L}_a, \\ \mathbf{B}_a &= -\mathbb{K}_{aa}^{-1} : \mathbf{L}_a,\end{aligned}\quad (27)$$

and resulting in

$$\mathbf{b}^{hom} = S \cdot \begin{bmatrix} \mathbf{B}_p \\ \mathbf{B}_a \end{bmatrix} = \begin{bmatrix} \mathbf{b}_p^{hom} \\ \mathbf{b}_a^{hom} \end{bmatrix}.\quad (28)$$

A similar procedure is applied for derivation of the effective Biot modulus, yielding

$$\frac{1}{N^{hom}} = \sum_{layer} f_{layer} \left( -\beta_a : \mathbb{C}_{aa}^{-1} : \mathbf{b}_a^{hom} + \beta_a : \mathbb{C}_{aa}^{-1} : \beta_a + \frac{1}{N_{layer}} \right).\quad (29)$$

The overall Biot modulus  $1/M^{hom}$  and the undrained stiffness  $\mathbb{C}^{hom,undrained}$  follow from  $\mathbb{C}^{hom,drained}$ ,  $\mathbf{b}^{hom}$  and  $N^{hom}$  according to Eqs. (13) and (14).

### 3. Poromicromechanical model for wood

The presented model builds up on a poromicromechanical approach to softwood elasticity by Bader *et al.* (2011). Herein, we extend this model by considering the layered structure of the cell wall, the restraining effect of ray cell bundles, and the laminate structure of the annual rings. The resulting six homogenization steps at five hierarchical levels are described in the following. An outline of the homogenization scheme is shown in Fig. 3, where also typical dimensions of RVEs and unit cells and their microstructures are specified.

#### 3.1 Polymer network

In homogenization step **Ia**, hemicelluloses (*HC*), lignin (*L*) and extractives (*EXT*) are combined to a polymer network including pores filled with water ( $\text{H}_2\text{O}$ ). This is accomplished by a self-consistent scheme with spherically-shaped inclusions, cylindrically and spherically-shaped pores, and an isotropic matrix, representing well the dispersed arrangement of the ingredients and the intimate mixing of polymers and water. Hence, the stiffness tensor  $\mathbb{C}^0$  is equal to  $\mathbb{C}_{poly,cwl}^{hom,drained}$  as described in Section 2.3. The assumption of cylindrical shape of the pore space is contrary to Bader *et al.* (2011). It allows to represent the preferred orientation of the polymers and, thus, also of the sorption sites along the cellulosic fibrils. Adopting a poromechanical framework (cf. Chapter 3 of (Bader *et al.* 2011)) results in a homogenized stiffness tensor  $\mathbb{C}_{poly,cwl}^{hom,drained}$  and poromechanical values  $\mathbf{b}_{poly,cwl}^{hom}$  and  $N_{poly,cwl}^{hom}$ . Specifying Eqs. (1), (2), (7) and (10) for volume fractions  $f_r$ , stiffness tensors  $\mathbb{C}_r$ , and Hill tensors  $\mathbb{P}_r^0$  (cf. (Bader *et al.* 2011)), of the mentioned phases results in

$$\mathbb{C}_{poly,cwl}^{hom,drained} = f_{HC} \mathbb{C}_{HC} : \mathbb{A}_{HC} + f_L \mathbb{C}_L : \mathbb{A}_L + f_{EXT} \mathbb{C}_{EXT} : \mathbb{A}_{EXT},\quad (30)$$

$$\mathbf{b}_{poly,cwl}^{hom} = f_{\text{H}_2\text{O}} \mathbf{1} : \mathbb{A}_{\text{H}_2\text{O}},\quad (31)$$

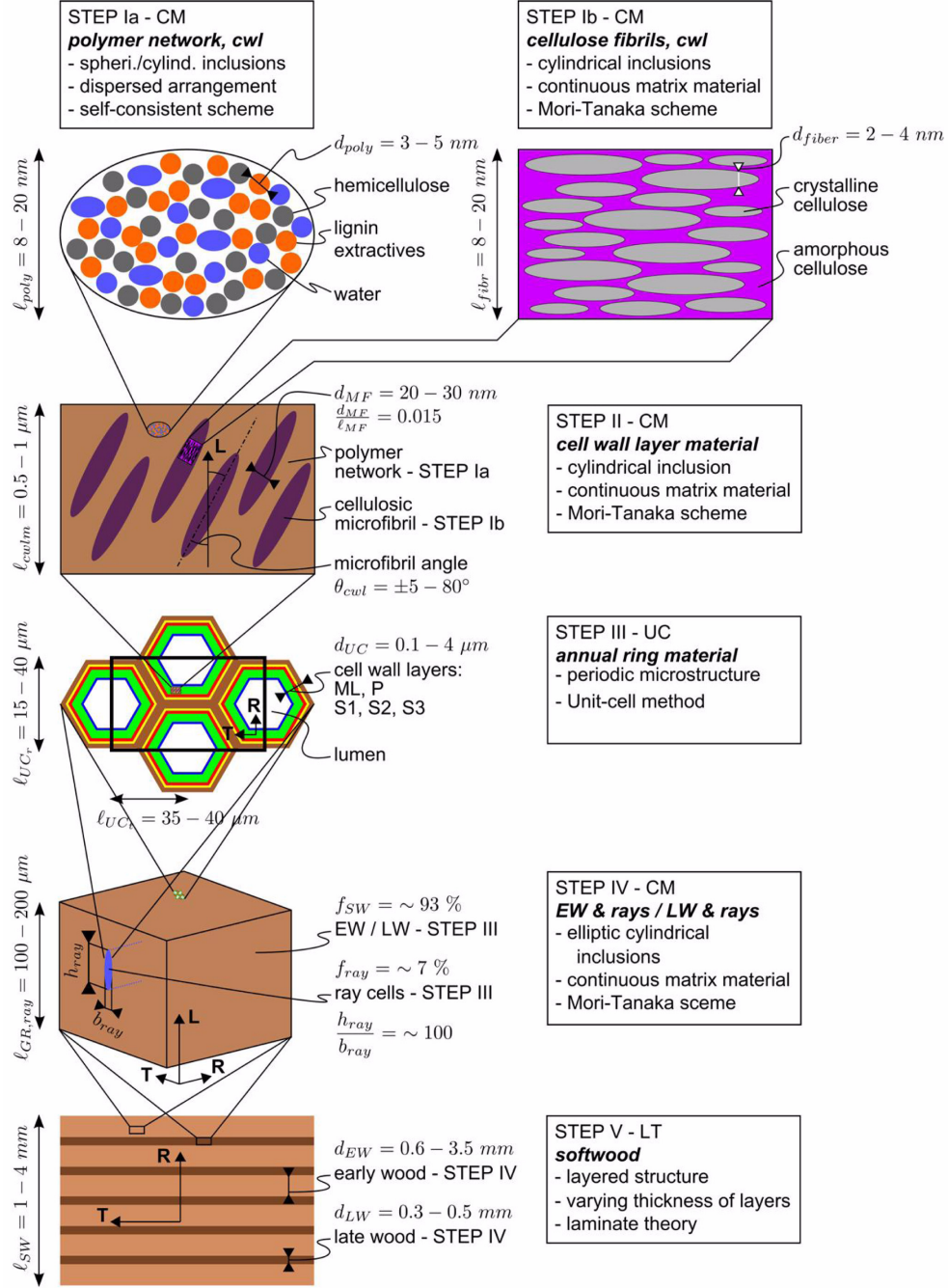


Fig. 3 Homogenization steps for softwood

$$\frac{1}{N_{poly,cwl}^{hom}} = f_{H_2O} \mathbf{1} : (f_{HC} \mathbb{A}_{HC} + f_L \mathbb{A}_L + f_{EXT} \mathbb{A}_{EXT}) : [\mathbb{I} - \mathbb{P}_{pore}^0 : \mathbb{C}^0]^{-1} : \mathbb{P}_{pore}^0 : \mathbf{1}. \quad (32)$$

This homogenization step is executed for each of the five cell wall layers ( $ML$ ,  $P$ ,  $S1$ ,  $S2$ ,  $S3$ ) of earlywood ( $EW$ ) and latewood ( $LW$ ) cells with different chemical compositions (cf. Table 1).

### 3.2 Cellulose fibrils

In homogenization step **Ib**, crystalline cellulose ( $CC$ ) is embedded into a matrix of isotropic amorphous cellulose ( $AC$ ) making up transversally isotropic inclusions. This results in a transversally isotropic material with the cylinder axis of the crystallites serving as axis of rotational symmetry. A Mori-Tanaka scheme is applied in a purely elastic framework (Zaoui 2002), since no pore space is assumed to exist in the cellulose fibrils, with stiffness of matrix material, amorphous cellulose, being  $\mathbb{C}^0$ . This step refers to the same length scale as step **Ia** for the polymer network. Specifying Eqs. (1) and (2) for volume fractions  $f_r$ , stiffness tensors  $\mathbb{c}_r$  of the listed phases yields

$$\mathbb{C}_C^{hom} = f_{CC} \mathbb{c}_{CC} : \mathbb{A}_{CC} + f_{AC} \mathbb{c}_{AC} : \mathbb{A}_{AC}. \quad (33)$$

Estimation of the concentration tensors  $\mathbb{A}_{CC}$ ,  $\mathbb{A}_{AC}$  and Hill tensor  $\mathbb{P}$  for each phase is done as shown in (Bader *et al.* 2011).

### 3.3 Cell wall layer material

In homogenization step **II**, the ellipsoid-shaped cellulose fibrils with stiffness  $\mathbb{C}_C^{hom}$  according to step **Ib** are embedded into the transversally isotropic polymer matrix with stiffness  $\mathbb{C}_{poly,cwl}^{hom,drained}$  derived in step **Ia**, resulting in the material of a cell wall layer. Varying chemical compositions are considered in steps **Ia** and **II** as well as different MFAs in step **II** for the different cell wall layers. The matrix-inclusion-type morphology of all five cell wall layers is suitably captured by a Mori-Tanaka scheme, with stiffness of matrix material, polymer network, being  $\mathbb{C}^0$ . Specifying Eqs. (1), (2), (7) and (10) for volume fractions  $f_r$ , stiffness tensors  $\mathbb{c}_r$  and Hill tensors  $\mathbb{P}_r^0$  (Bader *et al.* 2011) of the phases of this step (cf. (Bader *et al.* 2011)) results in

$$\mathbb{C}_{cwl}^{hom,drained} = f_{poly,cwl} \mathbb{c}_{poly,cwl} : \mathbb{A}_{poly,cwl} + f_{C,cwl} \mathbb{c}_C : \mathbb{A}_{C,cwl} \quad (34)$$

$$\mathbf{b}_{cwl}^{hom} = f_{poly,cwl} \mathbf{b}_{poly,cwl} : \mathbb{A}_{poly,cwl} \quad (35)$$

$$\frac{1}{N_{cwl}^{hom}} = \mathbf{b}_{cwl}^{hom} : f_{C,cwl} \{ [\mathbb{I} + \mathbb{P}_C^{poly} : (\mathbb{c}_C - \mathbb{c}_{poly}) ]^{-1} : \mathbb{P}_C^{poly} : \mathbf{b}_{poly} \} + f_{poly} \frac{1}{N_{poly}}. \quad (36)$$

Estimation of the concentration tensors  $\mathbb{A}$ , and Hill tensors  $\mathbb{P}$  for each phase is done as shown in (Bader *et al.* 2011). In contrast to Bader *et al.* (2011), the microfibrils are embedded only perpendicular to the thickness direction of the cell wall layer at an inclination defined by MFA (cf. Table 1) to the longitudinal axis in the cell wall layer plane. No different orientations in the transverse plane are considered. This results in transversally isotropic material behavior of each cell wall layer with an axis of rotational symmetry aligned with the cellulose microfibrils, except for layer  $S1$ , where crossed microfibrils in the cell wall layer plane result in an orthotropic material behavior. The different inclination angles in the different layers are considered at the next higher length scale by accordingly specifying the orientations of the principal material directions in each layer.

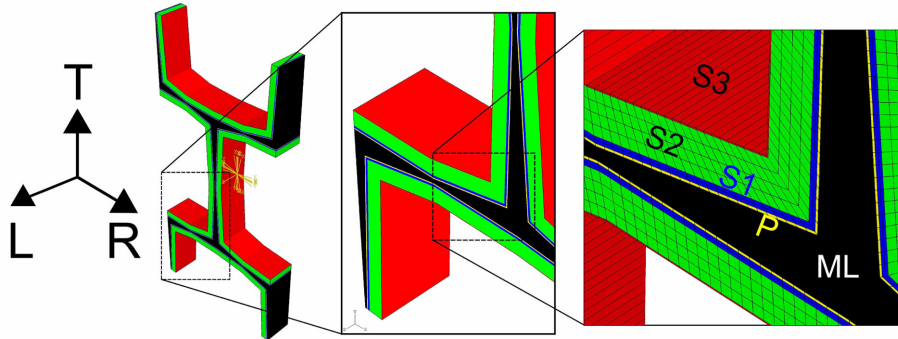


Fig. 4 Unit cell of wood cell structure for finite element calculation

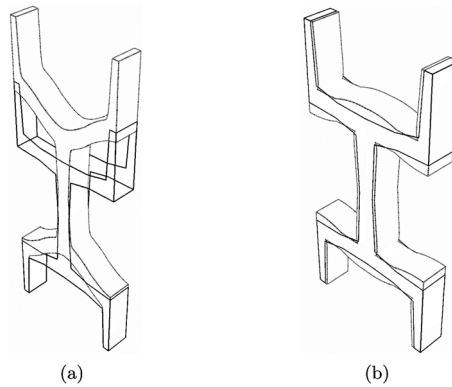


Fig. 5 Application of the unit cell method: Deformed state of a unit cell due to unit macroscopic strain  $E_{TT} = 1$  at otherwise restrained conditions in Fig. 5(a) and due to unit microscopic pressure  $p^{UC} = 1$  at totally restrained conditions in Fig. 5(b)

### 3.4 Earlywood and latewood

Homogenization step **III** deals with the cellular structure of wood, for which effective poroelastic quantities are derived by means of the unit cell method. It is executed numerically using the finite element method (commercial code ABAQUS, version 6.7). A double-Y shaped unit cell is chosen to approximate the cellular structure of wood, see Fig. 4. It is defined by the ratio of radial and tangential cell dimensions, cell wall layer thicknesses and the inclination of the radial cell walls. Due to the large extensions of the wood fibers in longitudinal direction compared to the dimensions in the transversal plane, the inspection of a thin cross-section plate is admissible. The walls are subdivided into four layers with parallel surfaces on each side of the middle lamella, which exhibits increasing thickness towards the cell wall crossings. The unit cell shows different dimensions for earlywood and latewood, cf. Tables 1 and 2. Different poromechanical properties are assigned to the various cell wall layers according to the results of the previous homogenization steps. As described in Subsection 2.3, application of various reference strain states allows to identify corresponding components of the drained stiffness tensor and the Biot tensor. In an exemplary manner, Fig. 5(a) shows the deformation state resulting from macroscopic strain state  $E_{TT} = 1$ , while  $E_{RR} = E_{LL} =$

$E_{RT} = E_{RL} = E_{TL} = 0$  and  $p = 0$ , which is used for determination of components  $C_{ijTT}$  of the drained stiffness tensor,  $ij = [LL, RR, TT, LR, RT, TL]$ . The according deformation state for determination of the poroelastic properties is shown in Fig. 5(b). Thereby, as described in Subsection 2.3, a unit pore pressure is applied, while all macroscopic strains are set to zero. The pore pressure results in a principal (shear stress-free) stress state in the cell wall which is determined numerically. Spatial averages of the obtained stresses over the volume of the unit cell  $\Sigma^{UC}$  equal the components of the Biot tensor  $\mathbf{b}_{SW}^{hom}$  of softwood, cf. Eq. (15). Evaluation of the porosity change yields directly the Biot modulus  $N_{SW}^{hom}$  of softwood, cf. Eq. (16). In a first approach, ray cells are considered purely elastically (water is treated as one solid phase of the polymer network) as radial reinforcement of earlywood and latewood. Effective elastic properties of ray cell bundles are derived in an analogous manner as for earlywood and latewood cells, but with different shape parameters and cell wall layer thicknesses.

### 3.5 Earlywood with rays / latewood with rays

In homogenization step **IV**, the orthotropic materials earlywood and latewood are interpenetrated in radial direction by ray cell bundles. Since typical dimensions of the ray cell bundles (approximately  $150 \mu\text{m}$ ) are well below typical widths of annual rings (approximately  $2 \text{ mm}$ ), the ray cell bundles are incorporated into the cellular wood material before earlywood and latewood are combined to the layered softwood. Since the decisive dimensions of these two homogenization steps are different ( $R$  for step **IV**,  $L$  and  $T$  for step **V**), these two steps are exchangeable without any effect on the final result (Eitelberger and Hofstetter 2011). In view of the embedment of the ray cell bundles in a continuous (cellular) matrix, a Mori-Tanaka scheme is applied, with stiffness of matrix material, earlywood or latewood, being  $\mathbb{C}^0$ . The shape parameters of ray cells are considered as constant for earlywood and latewood. Specifying Eqs. (1), (2), (7) and (10) for volume fractions  $f_r$ , stiffness tensors  $\mathbb{C}_r$ , and Hill tensors  $\mathbb{P}_r^0$  (Bader *et al.* 2011) of earlywood or latewood and ray cells, all from step **III**, one obtains exemplary for earlywood

$$\mathbb{C}_{EW_{ray}}^{hom, drained} = f_{EW} \mathbb{C}_{EW} : \mathbb{A}_{EW} + f_{ray} \mathbb{C}_{ray} : \mathbb{A}_{ray}, \quad (37)$$

$$\mathbf{b}_{EW_{ray}}^{hom} = f_{EW} \mathbf{b}_{EW} : \mathbb{A}_{EW}, \quad (38)$$

$$\frac{1}{N_{EW_{ray}}^{hom}} = \mathbf{b}_{EW} : f_{ray} \{ [\mathbb{I} + \mathbb{P}_{ray} : (\mathbb{C}_{ray} - \mathbb{C}_{EW}) ]^{-1} : \mathbb{P}_C^{EW} : \mathbf{b}_{EW} \} + f_{EW} \frac{1}{N_{EW}}. \quad (39)$$

Estimation of the concentration tensors  $\mathbb{A}$  and Hill tensors  $\mathbb{P}$  for each phase is done as shown in (Bader *et al.* 2011).

### 3.6 Softwood

In homogenization step **V**, the layers of earlywood ( $EW_{ray}$ ) and latewood ( $LW_{ray}$ ) reinforced by ray cell bundles, are combined by means of laminate theory. Thereby, the curvature of the annual rings is disregarded, as well as the continuous transition between earlywood and latewood. Rather a structure built of parallel alternating plane layers of earlywood and latewood is considered. The homogenized drained stiffness tensor  $\mathbb{C}_{SW}^{hom, drained}$ , the Biot tensor  $\mathbf{b}_{SW}^{hom}$  and the Biot modulus  $N_{SW}^{hom}$  follow from specifying Eqs. (18) and (20) to (29) for volume fractions  $f_r$ , stiffness tensors  $\mathbb{C}_r$ , Biot

tensors  $\mathbf{b}_r$ , and Biot moduli  $N_r$  for the described layers of earlywood and latewood with rays with properties according to step IV. The plane and antiplane parts of the drained stiffness tensor, of earlywood with rays read - using Eq. (18) - for example as

$$\mathbb{C}_{EW_{ray}}^{drained,sorted} = \mathcal{S}^T \cdot \mathbb{C}_{EW_{ray}}^{drained} \cdot \mathcal{S} = \begin{bmatrix} \mathbb{C}_{pp} & \mathbb{C}_{pa} \\ \mathbb{C}_{ap} & \mathbb{C}_{aa} \end{bmatrix}_{EW_{ray}}^{drained,sorted}. \quad (40)$$

The plane and antiplane tensor components of softwood according to Eq. (20) are averaged over the layers as described in Eq. (21)

$$\mathbb{K}_{ij,SW} = \sum_{AR=EW_{ray}}^{LW_{ray}} f_{AR} \mathbb{K}_{ij,AR} \quad i, j \in \{a, p\}. \quad (41)$$

Using Eqs. (22) and (23) for softwood yields the stiffness tensor  $\mathbb{C}_{SW_{ray}}^{hom,drained}$  and its plane and antiplane components, respectively, as

$$\mathbb{C}_{SW_{ray}}^{hom,drained} = \mathcal{S} \cdot \begin{bmatrix} \mathbb{C}_{pp} & \mathbb{C}_{pa} \\ \mathbb{C}_{ap} & \mathbb{C}_{aa} \end{bmatrix}_{SW_{ray}}^{drained,sorted} \cdot \mathcal{S}^T. \quad (42)$$

For the poromechanical equations this procedure is also applied to the second-order Biot tensor, whose plane and antiplane parts read, following Eq. (24), again exemplarily for earlywood, as

$$\beta_{EW_{ray}} = \mathcal{S}^T \cdot \mathbf{b}_{EW_{ray}} = \begin{bmatrix} \beta_p \\ \beta_a \end{bmatrix}_{EW_{ray}}. \quad (43)$$

Averaging over the layers following Eq. (25) yields

$$\mathbf{L}_{i,SW} = \sum_{AR=EW_{ray}}^{LW_{ray}} f_{AR} \mathbf{L}_{i,AR} \quad i \in \{a, p\}. \quad (44)$$

Specifying Eq. (27) for softwood, the homogenized Biot tensor (cf. Eq. (28)) and the homogenized Biot modulus (cf. Eq. (29)) read as

$$\mathbf{b}_{SW_{ray}}^{hom} = \mathcal{S} \cdot \begin{bmatrix} \mathbf{B}_p \\ \mathbf{B}_a \end{bmatrix} = \begin{bmatrix} \mathbf{b}_{SW_{ray,p}}^{hom} \\ \mathbf{b}_{SW_{ray,a}}^{hom} \end{bmatrix}, \quad (45)$$

$$\frac{1}{N_{SW_{ray}}^{hom}} = \sum_{AR=EW_{ray}}^{LW_{ray}} f_{AR} \left( -\beta_{a,AR} : \mathbb{C}_{aa,AR}^{-1} : \mathbf{b}_{SW_{ray,a}}^{hom} + \beta_{a,AR} : \mathbb{C}_{aa,AR}^{-1} : \beta_{a,AR} + \frac{1}{N_{AR}} \right). \quad (46)$$

In wood, generally undrained conditions are observed under the fiber saturation point. The undrained stiffness tensor follows from

$$\mathbb{C}_{SW_{ray}}^{hom,undrained} = \mathbb{C}_{SW_{ray}}^{hom,drained} + M_{SW_{ray}}^{hom} : \mathbf{b}_{SW_{ray}}^{hom,T} : \mathbf{b}_{SW_{ray}}^{hom}, \quad (47)$$

$$\text{where } \frac{1}{M_{SW_{ray}}^{hom}} = \frac{\phi_{0,SW}}{k_{H_2O}} + \frac{1}{N_{SW_{ray}}^{hom}}. \quad (48)$$

$\phi_{0,SW}$  equals the volume fraction of water in softwood (cf. Section 4).  $k_{H_2O}$  stands for the bulk modulus of water, assuming a linear constitutive relationship for water.

#### 4. Physical and chemical properties of moisturized softwood

In order to evaluate the multiscale model, the volume fractions of the phases of all homogenization steps have to be determined. We consider mass density and moisture content as sample-specific independent properties, while we use typical values for a particular wood species, namely spruce, reported in the literature for chemical composition, cell wall layer thicknesses, and ratios of densities of earlywood and latewood. In the following, the determination of the volume fractions of the phases in each homogenization step is sketched. For this purpose, some considerations on densities are required first.

##### 4.1 Wood densities

The density of a wood sample is generally specified in the wet state, i.e., the state in equilibrium with the surrounding environment. For determination of the volume fractions in the multiscale model, we need to derive therefrom the individual densities of earlywood and latewood. Obviously, this requires some assumptions on the annual ring structure. We make use of a constant density ratio of earlywood and latewood and a density-dependent latewood fraction. The latter was specified by Lindström (1996) for Norway spruce based on statistical analysis of density measurements as

$$f_{LW, dry}^{SW} = 1.0811 \cdot \rho_{SW_{ray, dry}} - 0.2703, \quad (49)$$

$$f_{EW, dry}^{SW} = 1 - f_{LW, dry}^{SW}. \quad (50)$$

The involved dry mass density of softwood follows from the corresponding volume in the wet state and the moisture content  $MC$ , specified in wood technology as mass of water related to the mass of the dry cell wall, of the sample according to Kollmann (1951) as

$$\rho_{SW_{ray, dry}} = \rho_{SW_{ray, wet}} \cdot \frac{1}{1 + MC - 0.84 \cdot \rho_{SW_{ray, wet}} \cdot MC}. \quad (51)$$

The softwood densities mentioned in literature contain densities of earlywood, latewood and ray cell bundles subjected to their volume fractions in softwood. Using the quantities from Table 3

Table 3 Typical characteristics of softwood (Fengel and Wegener 1983, Kollmann 1951, Wagenführ 2007), used in the model ( $\rho_{wet}$  specified for  $MC = 12\%$ )

	$\rho_{wet}$	$\rho_{dry}$	$f$
	[g/cm <sup>3</sup> ]	[g/cm <sup>3</sup> ]	[%]
Softwood	~0.46	~0.43	~93
Ray cell bundles	~0.33	~0.30	~7
Softwood + ray cell bundles	~0.45	~0.42	100

and Eq. (51) the density of softwood without ray cells read as

$$\rho_{SW, dry} = \frac{\rho_{SW, ray, dry} - f_{ray} \cdot \rho_{ray, dry}}{f_{SW}}. \quad (52)$$

Finally, assuming a ratio between earlywood and latewood density in the dry state of  $\rho_{LW/EW} =$

$\frac{\rho_{LW, dry}}{\rho_{EW, dry}} = 2.60$  following Kollmann (1951) and Lindström (1996), the sought densities of these two tissues

read in the dry state as

$$\rho_{EW, dry} = \frac{\rho_{SW, dry}}{f_{EW, dry}^{SW} + f_{LW, dry}^{SW} \cdot \rho_{LW/EW}} \quad (53)$$

$$\rho_{LW, dry} = \rho_{LW/EW} \cdot \rho_{EW, dry}. \quad (54)$$

#### 4.2 Determination of microscopic to macroscopic volume fractions of components in dry state

We emanate from weight fractions for the chemical constituents (*CC*, *AC*, *HC*, *L* and *EXT*) in the dry state of the cell wall layers (cf. Table 1) and derive their volume fractions across all length scales in the dry state therefrom. Afterwards, the water is distributed from a given macroscopic *MC* down to the scale of the cell wall layer matrix, considering the sorption capacities of the different polymers. Finally, volume fractions in the wet state are derived. A crystalline fraction of 66% in volume is assumed for cellulose (Fengel and Wegener 1983).

In the following the index *chem* is used for the chemical components (*CC*, *AC*, *HC*, *L*, *EXT*),  $c_{wl}$  for the cell wall layers, and  $c_w$  for the cell wall of earlywood *EW*, latewood *LW* and softwood *SW*. Wet and dry states are indicated by *wet* and *dry*, respectively. Subscripts refer to particular components, and superscripts to the length scale.

##### 4.2.1 Chemical composition in dry state at the meso scale - cell wall layers

From the weight fractions of the wood polymers in each cell wall layer in earlywood and latewood, respectively (Table 1 and (Bergander 2001, Persson 2000, Fengel and Wegener 1983, Kollmann 1951, Qing and Mishnaevsky 2008)), their corresponding volume fractions at the same length scale are calculated by means of their densities  $\rho_{chem}$  (Hofstetter *et al.*, 2006). This results exemplarily for a particular cell wall layer of earlywood in

$$f_{chem, dry}^{EW, cwl} = w f_{chem, dry}^{EW, cwl} \cdot \frac{\rho_{cwl, dry}^{EW}}{\rho_{chem}} \quad \text{where} \quad \rho_{cwl, dry}^{EW} = \frac{1}{\sum_{chem} \frac{w f_{chem, dry}^{EW, cwl}}{\rho_{chem}}}. \quad (55)$$

##### 4.2.2 Chemical components in dry state at the meso scale - cell walls of earlywood and latewood

The volume fraction of each chemical component at cell wall scale is derived from its respective fraction in each cell wall layer, by a weighted sum over all layers, with volume fractions computed from ratios of cross-sectional areas as

$$f_{chem, dry}^{EW, cw} = \sum_{cwl} f_{chem, dry}^{EW, cwl} \cdot f_{chem, dry}^{EW, cw} \quad \text{where} \quad f_{cwl, dry}^{EW, cw} = \frac{A_{cwl, dry}^{EW}}{\sum_{cwl} A_{cwl, dry}^{EW}}. \quad (56)$$

Volume fractions of the chemical components of the ray cell tissue are assumed to be averaged over earlywood and latewood tissues, and are thus not mentioned in Eq. (56). The cross-sectional areas of the cell wall layers are obtained from the previous calculations for the finite element model for the different unit cells. Corollary all these steps are done for latewood. The volume fraction of each chemical component at the wood cell scale in earlywood reads as

$$f_{chem, dry}^{EW} = f_{chem, dry}^{EW, cw} \cdot f_{cw, dry}^{EW}, \quad (57)$$

with

$$f_{cw, dry}^{EW} = \frac{\rho_{EW, dry}^{EW}}{\rho_{cw, dry}^{EW}} \quad \text{and} \quad f_{lum, dry}^{EW} = 1 - f_{cw, dry}^{EW}. \quad (58)$$

Therein, the density of earlywood follows from Eq. (53) and the cell wall density as

$$\rho_{cw, dry}^{EW} = \sum_{chem} f_{chem, dry}^{EW, cw} \cdot \rho_{chem}. \quad (59)$$

#### 4.2.3 Chemical components in dry state at the macroscale -softwood

Finally, the volume fractions at the macroscale are obtained by considering the volume fractions of earlywood and latewood in the tissue in the dry state (cf. Eqs. (49) and (50)) as

$$f_{chem, dry}^{SW} = f_{chem, dry}^{EW} \cdot f_{EW, dry}^{SW} + f_{chem, dry}^{LW} \cdot f_{LW, dry}^{SW}. \quad (60)$$

#### 4.3 Distribution of moisture

The water split-up is done dependent on the sorption capacities of hemicellulose, lignin and cellulose with its crystalline and amorphous parts. Smith and Langrish (2008) summarized the sorption capabilities of these chemical wood components, described in Table 4. In this table, also the fractional sorptive capacity relative to wood in the model is specified which follows for a given chemical composition from

$$SC_{chem} = \frac{f_{chem, dry}^{SW} \cdot SC_{chem}^{SW}}{\sum_{chem} f_{chem, dry}^{SW} \cdot SC_{chem}^{SW}}. \quad (61)$$

The sorption capacities of the various cell wall layers control the water distribution. As for the sorptive capacities of the single wood polymers, these capacities are specified for the dry material. With the sorption capacities  $SC_{chem}$  from Table 4 and the calculated component volume fractions  $f_{chem, dry}^{EW/LW, cwl}$  from Eq. (55) the sorption capacities of the cell wall layers  $SC_{cwl, dry}^{EW/LW}$ , exemplary for earlywood, read as

$$SC_{cwl, dry}^{EW} = \sum_{chem} SC_{chem} \cdot f_{chem, dry}^{EW, cwl}. \quad (62)$$

Table 4 Sorptive capacity of individual components of wood (Smith and Langrish 2008)

Chemical component	Volume fraction $f_{chem,dry}^{SW}$	Sorptive capacity relative to wood $sc_{chem}^{SW}$	Fractional sorptive capacity relative to wood in the model
	[%]	[%]	[%]
Cellulose	$42 \pm 2$	0,94	$sc_C = 0,40$
Hemicelluloses	$27 \pm 2$	1,56	$sc_{HC} = 0,43$
Lignin	$28 \pm 3$	0,60	$sc_L = 0,17$
Extractives	$3 \pm 2$	0,00	$sc_{EXT} = 0,00$
Wood	100		$sc_{SW} = 1,00$

The total volume of water to be distributed in the wood tissue related to the volume of the solid substance, i.e., the cell walls, in the dry state reads as

$$H_2O_{dry}^{SW} = MC \cdot \frac{\rho_{cw,dry}^{SW}}{\rho_{H_2O}}, \quad (63)$$

where the average of the earlywood and latewood cell wall densities at dry state reads as

$$\rho_{cw,dry}^{SW} = \rho_{cw,dry}^{EW} \cdot f_{cw,dry}^{EW} \cdot f_{EW,dry}^{SW} + \rho_{cw,dry}^{LW} \cdot f_{cw,dry}^{LW} \cdot f_{LW,dry}^{SW}. \quad (64)$$

Therefrom, the water fraction in a cell wall layer follows from

$$H_2O_{EW,cwl,dry}^{SW} = H_2O_{dry}^{SW} \cdot \frac{sc_{dry}^{EW,cwl} \cdot f_{cwl,dry}^{EW} \cdot f_{EW,dry}^{SW}}{\sum_{GR=EW} \left( \sum_{cwl} sc_{dry}^{GR,cwl} \cdot f_{cwl,dry}^{GR} \right) \cdot f_{GR,dry}^{SW}}. \quad (65)$$

$$H_2O_{cwl,dry}^{EW} = H_2O_{EW,cwl,dry}^{SW} \cdot \frac{1}{f_{EW,dry}^{SW}} \cdot \frac{1}{f_{cwl,dry}^{EW}}. \quad (66)$$

All these volume fractions are related to dry substance. The relation to wet substance and the determination of the volume fractions for the RVEs of the multiscale model are dealt with next.

#### 4.4 Volume fractions of homogenization steps (wet state)

The volume fractions of the chemical components in each cell wall layer in the wet state,  $f_{chem,cwl,wet}^{EW}$  read as

$$f_{chem,wet}^{EW,cwl} = \sum_{chem} \frac{f_{chem,dry}^{EW,cwl}}{f_{chem,dry}^{EW,cwl} + H_2O_{dry}^{EW,cwl}} \quad \text{and} \quad f_{H_2O,wet}^{EW,cwl} = \frac{H_2O_{dry}^{EW,cwl}}{\sum_{chem} f_{chem,dry}^{EW,cwl} + H_2O_{dry}^{EW,cwl}}, \quad (67)$$

$$\Rightarrow \sum_{chem} f_{chem,wet}^{EW,cwl} + f_{H_2O,wet}^{EW,cwl} = 1. \quad (68)$$

In a simplifying manner, the whole water fraction is considered in homogenization step **Ia**, where it is added to the chemical components hemicellulose, lignin and extractives. The failure to resolve

the water adsorbed by the amorphous fraction of cellulose only results in minor inaccuracies. The resulting volume fractions, exemplary for hemicellulose in a cell wall layer of earlywood, read as

$$f_{HC,wet}^{EW,cwl,poly} = \frac{f_{HC,wet}^{EW,cwl}}{f_{HC,wet}^{EW,cwl} + f_{L,wet}^{EW,cwl} + f_{H_2O,wet}^{EW,cwl} + f_{EXT,wet}^{EW,cwl}}. \quad (69)$$

In homogenization step **Ib**, the volume fractions of the crystalline and amorphous parts of cellulose read according to the given crystallinity ratio as  $f_{CC} = 66\%$  and  $f_{AC} = 34\%$ , for all cell wall layers and for earlywood and latewood.

At the length scale of the cell wall material the volume fractions of the polymer matrix  $f_{poly,cwl}$  and of the cellulose  $f_C$  compound in homogenization step **II** follow directly from Eq. (67) as

$$f_{poly,wet}^{EW,cwl} = f_{HC,wet}^{EW,cwl} + f_{L,wet}^{EW,cwl} + f_{H_2O,wet}^{EW,cwl} + f_{EXT,wet}^{EW,cwl}, \quad (70)$$

$$f_{C,wet}^{EW,cwl} = f_{CC,wet}^{EW,cwl} + f_{AC,wet}^{EW,cwl}. \quad (71)$$

In homogenization step **III** (unit cell method), the volume fraction of each cell wall layer is dependent on the geometry of the cell type - earlywood or latewood - and on the cell wall layer thickness. Using radial and tangential dimensions,  $\ell_R$  and  $\ell_T$  inclination of the radial cell wall  $\varphi$ , the broadening of the cell walls  $\beta$  (cf. Table 2), and the cell wall layer thicknesses (cf. Table 1), the geometry of earlywood and latewood cells are constructed. Varying the thickness of cell wall layer  $S_2$  leads to predetermined densities.

Considering homogenization step **IV**, in which earlywood and latewood are intersected by ray cells, the volume fractions specified in Table 3 are used

$$f_{EW/LW}^{SW_{ray}} = f_{softwood}, \quad (72)$$

$$f_{ray}^{SW_{ray}} = f_{ray \text{ cell bundles}}. \quad (73)$$

The poromechanical behavior resulting from step **IV** is used when merging earlywood and latewood in step **V**. According volume fractions for the laminate theory come from Eqs. (49) and (50). Additionally using Eqs. (56), (57), (58), (59) and (64) in the wet state, the volume fraction of the softwood lumen is calculated by

$$f_{lum,wet}^{SW} = 1 - \frac{\rho_{SW,wet}^{SW}}{\rho_{cw,wet}}. \quad (74)$$

## 5. Poromechanical values of softwood

### 5.1 Model limits

The poromechanical approach is suitable in ranges of moisture contents between 5 and 20%. Below that, molecular effects become dominant which are not represented in the model. Above a moisture content of 20%, partial condensation of the water in the lumens at the tracheid ends might

occur. Also this effect is not covered in the proposed approach. Moreover, the model is restricted to linearity and, thus, to small changes of the moisture content.

### 5.2 Model results

In order to demonstrate the functionality of the model, predictions for effective drained stiffness tensor components (Figs. 6(a) to 8(b)) as well as for effective Biot tensor components (Figs. 9(a) to 9(c)) and effective Biot moduli (Fig. 10) for softwood as well as for separate earlywood and latewood are presented. They were derived for typical microstructural characteristics of spruce and varying densities and moisture contents, expressed in terms of volume fractions of lumens and of water at the macroscopic scale, see Tables 1, 2 and 3. The used elasticity constants in the first homogenization steps are the same as described in (Bader *et al.* 2011). The results for only earlywood and only latewood are depicted in order to elucidate the influence of the annual rings. As shown in Fig. 6(a), stiffness in radial direction is controlled by the serial arrangement of earlywood and latewood. Continuous radial cell walls throughout the layers are responsible for load transfer in this direction. Tangential stiffness (cf. Fig. 6(b)) is very small in earlywood, since load transmission is based on bending of the radial cell walls in this case. Despite its low volume fraction, latewood is almost exclusively responsible for the stiffness in this direction. This effect results from the small lumen diameters in radial direction and the high cell wall thicknesses in latewood, activating shear and frame effects in transverse load transfer. Longitudinal stiffness (cf. Fig. 6(c)) is mainly influenced by the volume fractions of earlywood and latewood, respectively, and the microfibril

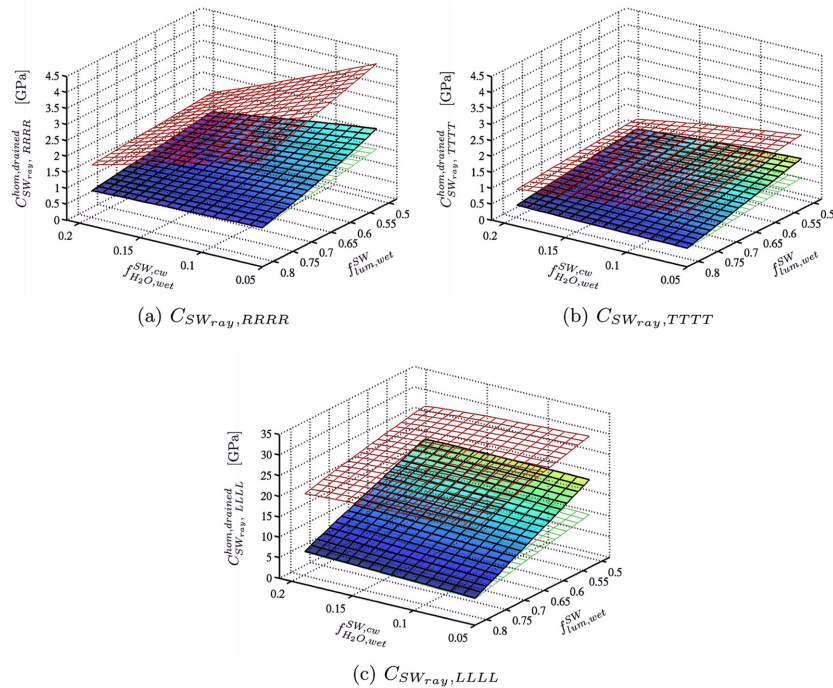


Fig. 6 Characteristics of the poromechanical model for softwood: Components of the drained stiffness tensor of softwood (middle surface), of earlywood (lower lines) and of latewood (upper lines) as function of the lumen volume fraction,  $f_{lum, wet}^{SW}$ , and of the cell wall-related volume fraction of water,  $f_{H_2O, wet}^{SW, cw}$ , typical for spruce

angle of the  $S2$ -layer. Because of the low values of the latter (cf. Table 2) and the dominant role of the  $S2$ -layer, the very stiff microfibrils considerably raise the longitudinal stiffnes.

Figs. 7(a) to 7(f) show the characteristics of the remaining stiffness tensor components. The shear stiffnesses related to the  $L$ -direction show a qualitatively similar behavior as the transversal axial

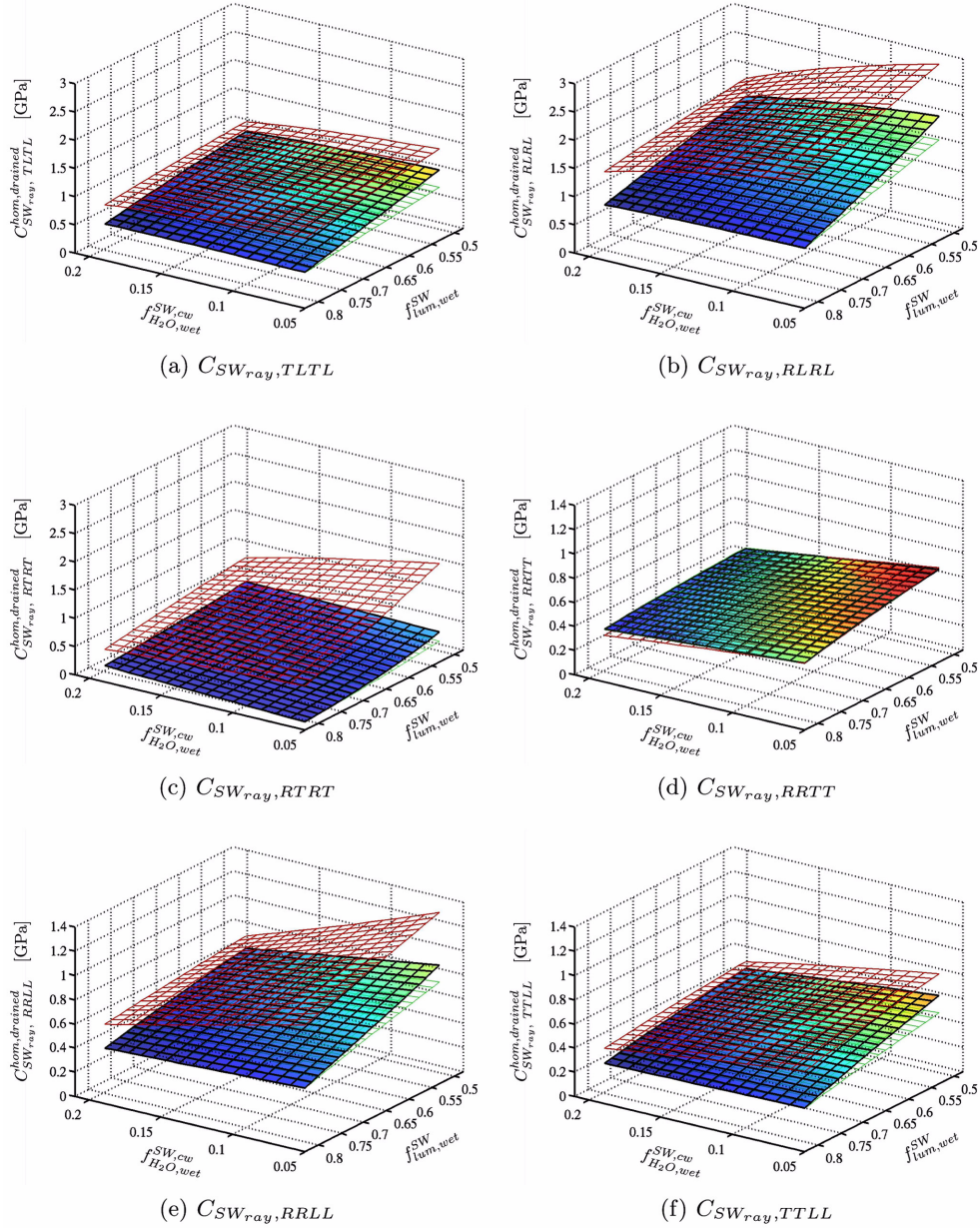


Fig. 7 Characteristics of the poromechanical model for softwood: Components of the drained stiffness tensor of softwood (middle surface), of earlywood (lower lines) and of latewood (upper lines) as function of the lumen volume fraction,  $f_{lum,wet}^{SW}$ , and of the cell wall-related volume fraction of water,  $f_{H_2O,wet}^{SW,cw}$ , typical for spruce

stiffnesses. In transversal direction, shear stiffness of softwood is very low, mainly caused by the low transversal shear stiffness of earlywood. Due to the layered structure of wood, the earlywood layers are dominant then.

As mentioned in Subsection 2.1, ray cells have a reinforcing influence in radial direction as shown in Figs. 8(a) to 8(c) depicting the stiffness tensor components  $C_{RRRR}$ ,  $C_{TTTT}$  and  $C_{LLLL}$  with and without consideration of wood rays. The longitudinal stiffness tensor component, on the contrary, is reduced due to the low transversal stiffness of the ray cells. The stiffness reduction effect of rays in the tangential direction is much lower due to the elliptical shape of the cross-section of the ray cell bundles with considerably lower extension in tangential than in longitudinal direction.

Figs. 9(a) to 9(c) show courses of the Biot tensor components  $b_{RR}$ ,  $b_{TT}$  and  $b_{LL}$  depending on volume fractions of water at the cell wall scale and lumens at the macroscale. Theoretical experiments have shown that a low inclination angle  $\varphi$  between radial and tangential cell wall results in a high radial and a low tangential Biot tensor component. In the tangential direction, the low bending stiffness of the cell walls, particularly in earlywood, results in little effect of eigenstresses in the cell walls.

Figs. 9(a) to 9(c) show consistently the highest Biot tensor components at high volume fractions of water and low volume fractions of lumens, meaning a high density, thick walls and a high stiffness. Pressure inside the water pores at low porosity (low values of  $f_{lumen,SW}$ ) results in high eigenstress of the cell wall material and - in spite of the decreasing stiffness with increasing water

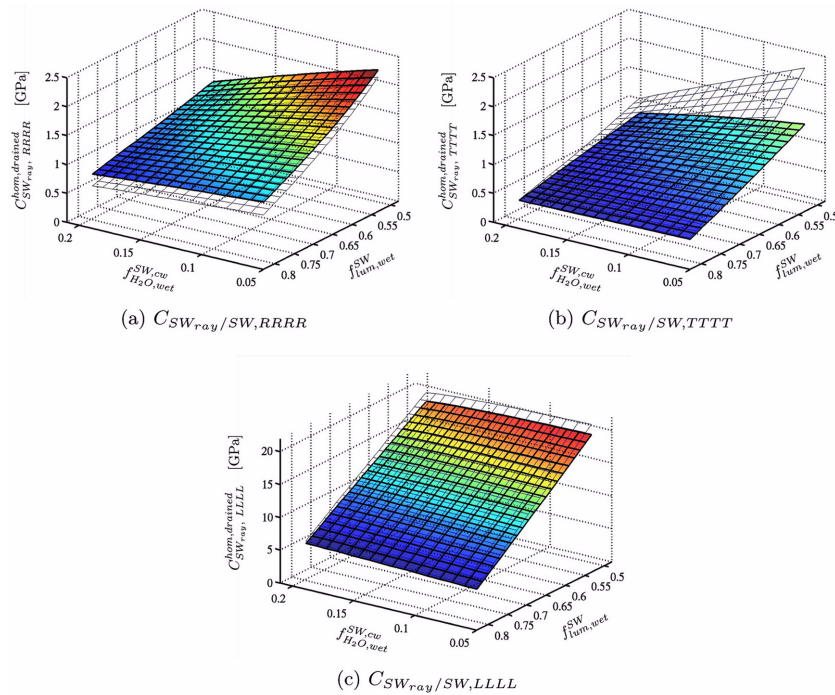


Fig. 8 Characteristics of the poromechanical model for softwood: Components of the drained stiffness tensor of ray restrained softwood (surface), and of softwood without rays (lines) as function of the lumen volume fraction,  $f_{lum, wet}^{SW}$ , and of the cell wall-related volume fraction of water,  $f_{H_2O, wet}^{SW, cw}$ , typical for spruce

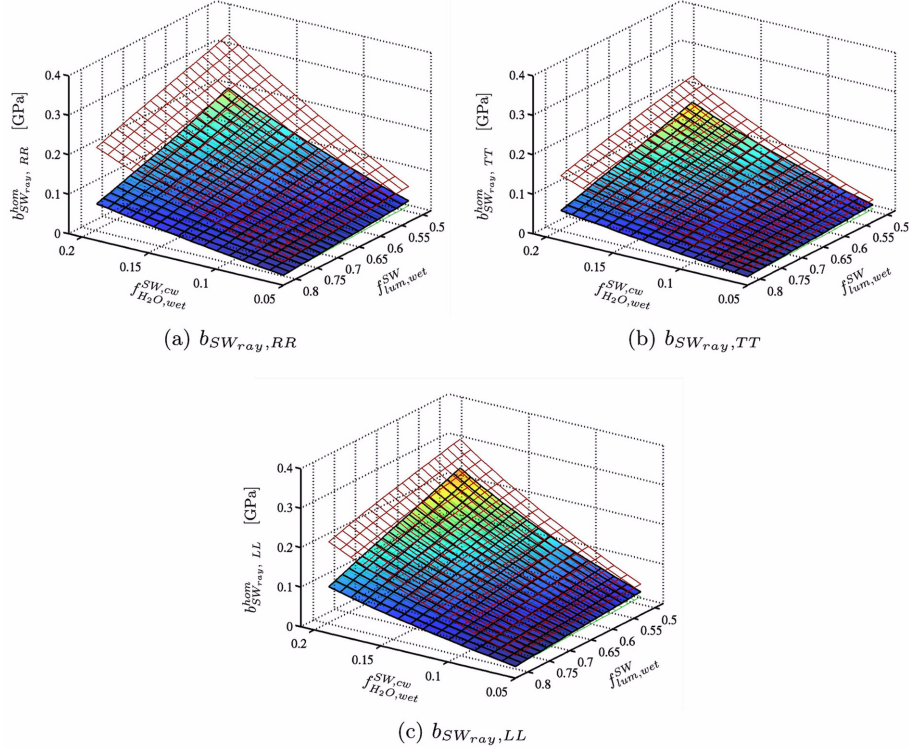


Fig. 9 Characteristics of the promechanical model for softwood: Components of the Biot tensor components of softwood (middle surface), of earlywood (lower lines) and of latewood (upper lines) as function of the lumen volume fraction,  $f_{lumen, wet}^{SW}$ , and of the cell wall-related volume fraction of water,  $f_{H_2O, wet}^{SW, cw}$ , typical for spruce

content - high macroscopic stresses and Biot tensor components, respectively. For lower density (high values of  $f_{lumen, SW}$ ) this effect decreases because of the decreasing stiffness of the material in all three principal material directions  $R$ ,  $T$  and  $L$ , resulting in higher deformations normal to the stiffness of the cell wall due to the eigenstresses.

The inverse of the effective Biot modulus  $\frac{1}{N_{SW_{ray}}}$  (cf. Fig. 10), which links pore pressure and change of porosity, shows a similar course as the Biot tensor components. At high water content the stiffness of the cell wall material declines due to the higher pore space. Thus, pressure in the water pores produces high volumetric changes of the pore space and, consequently, high values of  $\frac{1}{N_{SW_{ray}}}$ .

### 5.3 Validation -elastic moduli

The validation of this model is done by a comparison of elastic moduli with experimentally measured ones at the softwood level. First, data by Neuhaus (1981) experimentally determined for elastic moduli in radial, tangential and longitudinal direction of spruce wood ( $\rho_{SW, dry} = 0,417 \text{ g/cm}^3$ ) at different moisture contents are used. Herein, only values in the range of validity of the model in relation to the moisture content ( $MC = 5\text{--}20\%$ ) are considered. The spruce samples used in the

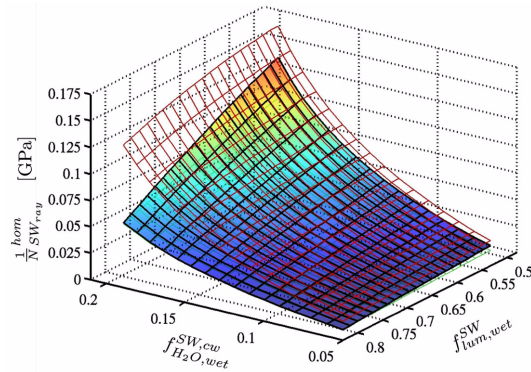


Fig. 10 Characteristics of the poromechanical model for softwood: Biot modulus of softwood (surface), of earlywood (lower lines) and of latewood (upper lines) as function of the lumen volume fraction,  $f_{lum, wet}^{SW}$ , and of the cell wall-related volume fraction of water,  $f_{H_2O, wet}^{SW, cw}$ , typical for spruce

experiments by Neuhaus show a low density. For their simulation by the multiscale model, the input parameters listed in Table 5 were applied. Densities of earlywood and latewood are related by

$\frac{rho_{LW}}{rho_{EW}} = 2.60$ , cf. Kollmann (1951). To compare the output of the model with the test results, the elastic moduli are computed from the stiffness tensor components. On the whole, a good agreement of experimental and numerical data is observed.

Fig. 11(a) shows a comparison of experimentally and numerically obtained longitudinal elastic moduli. The deviations between the model predictions and the experimental values probably result from simplifications in the representation of the chemical components in the model: For example, consideration of anisotropic shape and stiffness of amorphous cellulose and of cross-linking between the wood polymers would increase the model predictions for longitudinal stiffness (Hofstetter *et al.* 2006). Moreover, assuming ellipsoidal shape of the cellulose microfibrils instead of a cylindrical one would lead to a better agreement of the decreasing stiffness with increasing moisture content in line with values from literature. According improvements of the multiscale model are subject to future research. As for the radial and tangential directions, results of experiments and simulations match particularly well (see Fig. 11(b)).

Moreover, literature data on the relative change of elastic moduli in different material directions with moisture content are evaluated. A comparison between these measured courses and corresponding model predictions, all related to a moisture content of  $MC = 12\%$ , yields a good agreement as well (see Figs. 12(a), 12(b) and 12(c)). The inclination of the curve for the elastic modulus in longitudinal direction (Fig. 12(a)) strongly depends on the shape of the microfibrils. In radial (Fig. 12(b)) and in tangential (Fig. 12(c)) direction, microfibril angles, volume fractions of spherical and ellipsoidal pores, the inclination angle of the radial cell walls, the widening angle of the cell walls, and the volume fraction and the density of the ray cells take effect on the rate of decrease of the moduli.

Finally, data on ranges of elastic properties of softwood are collected from the literature and compared with results of the multiscale model, derived for typical ranges of microstructural characteristics (cf. Table 6). Again, a good agreement is observed.

The extension of the model by Bader *et al.* (2011) by differentiating earlywood and latewood

Table 5 Characteristics of earlywood, latewood, ray cells and softwood used for comparison with Neuhaus (1981)

	$\rho_{dry}$	$f$		cell diameter		$\varphi$	$\beta$
		EW/LW	SW/ray	R	T		
	[g/cm <sup>3</sup> ]	[%]	[%]	[ $\mu$ m]	[ $\mu$ m]	[ $^{\circ}$ ]	[ $^{\circ}$ ]
Earlywood	0.33	83		35	30	22	2
Latewood	0.84	17		28	30	6	1
Softwood	0.41	100	92.7				
Ray cells	0.30		7.3	40	30	13	10
Softwood and ray cells	0.40		100				

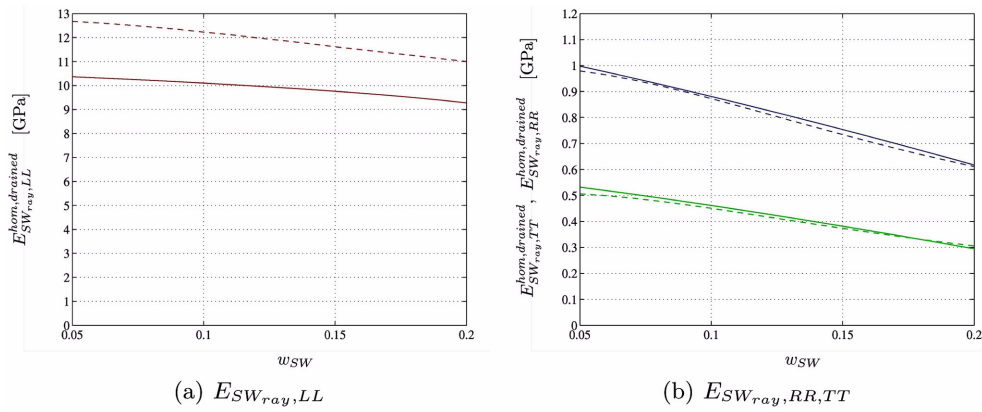


Fig. 11 Characteristics of the poromechanical model for softwood (continuous line) and comparison with Neuhaus (1981) (dashed line): Components of the drained elastic moduli of spruce for radial (top right), tangential (down right) and longitudinal (left figure) as function of the moisture content,  $w_{H_2O,SW}$ , typical for spruce

enables to explicitly consider additional anatomical characteristics, such as different cell shapes and cell wall compositions in earlywood and latewood. This increases the accuracy of the model predictions. Moreover, the implementation of ray cells results in more suitable predictions of the stiffness in radial direction, which also affects the ratio between the hygroexpansion coefficients in radial and tangential direction.

Because of the easy change of the anatomical characteristics, the model can be applied also to other softwood species. To simulate hardwood, only small adjustments such as inclusion of vessels in the model are necessary.

## 6. Coefficients of swelling and shrinkage of wood

### 6.1 Upscaling of microscale pressures

Upon swelling under increased relative humidity of the environment, water is incorporated in the cell wall matrix and exerts a swelling pressure  $\Pi^{sw}$ . This pressure is assumed to be isotropic, i.e.,  $\Pi^{sw} = \Pi^{sw} \mathbf{1}$  with  $\mathbf{1}$  denoting the second-order unity tensor. The resulting pore pressure  $p^{sw}$  is equal

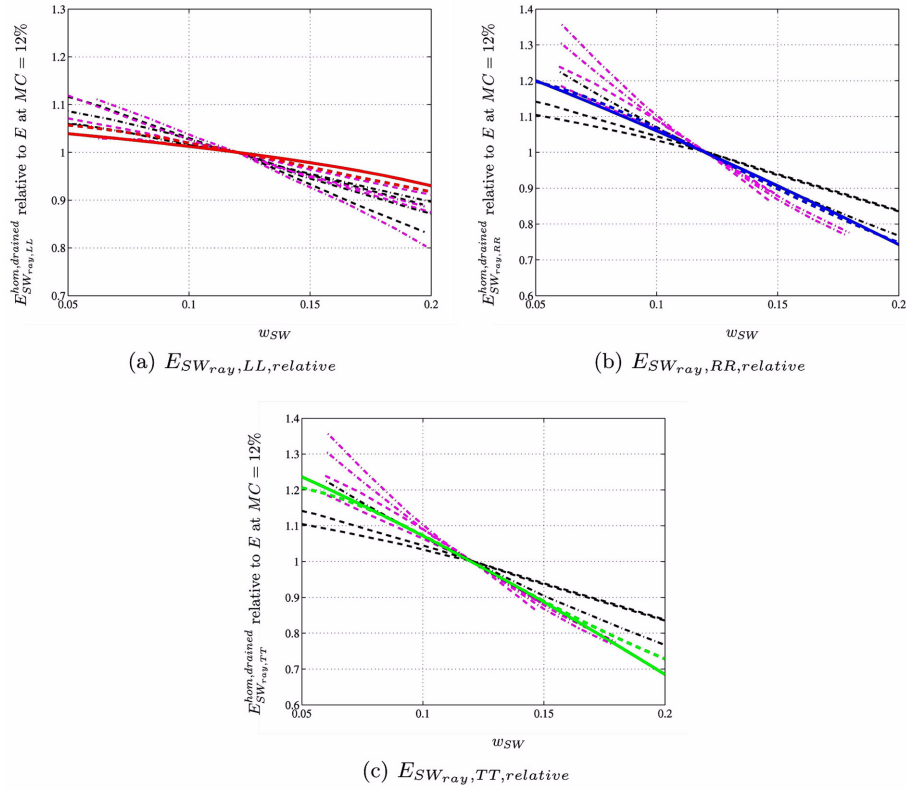


Fig. 12 Relative characteristics of the poromechanical model for softwood (continuous line) and comparison with (Neuhaus 1981, Schneider 1971, Kufner 1978, Wilson 1932, Sulzberger 1953, Kadita *et al.* 1961, Greenhill 1936, Siimes 1967, Elwood 1954): Components of the drained elastic moduli of spruce for radial, tangential, and longitudinal as function of the moisture content,  $w_{H_2O,SW}$ , typical for spruce

Table 6 Stiffness values of spruce earlywood and latewood, calc. stands for calculated, exp. stands for experimental results, (Moden and Berglund 2008b,a, Watanabe *et al.* 2002, Farruggia and Perré 2000)

	$SW_{ray}$	$EW_{ray}$		$LW_{ray}$		Investigation
	$\rho$	$E_{RR}$	$E_{TT}$	$E_{RR}$	$E_{TT}$	
	[g/cm <sup>3</sup> ]	[MPa]	[MPa]	[MPa]	[MPa]	
Spruce	0.39	532	65	5103	1336	calc.
Spruce	0.40	600-1500	-	1000-3000	-	exp.
Softwoods		200-1200	50-400	-	-	exp.
Spruce, ( $EW/LW$ )	0.30/0.75	740-800	160-230	-	1200-1250	exp.
Spruce, $MC = 5\%$	0.27-0.67 <sub>wet</sub>	430-950	130-380	2970-3850	1800-2630	model
Spruce, $MC = 12\%$	0.45 <sub>wet</sub>	500	170	2400	1600	model
Spruce, $MC = 20\%$	0.30-0.71 <sub>wet</sub>	300-550	90-210	1470-1720	930-1250	model

to the sum of the swelling pressure  $\Pi^{sw}$  and the pressure induced by elastic deformations of the surrounding solid material, expressed by an (isotropic) pressure  $p$

$$p_{pore}^{sw} = (p + \Pi^{sw})_{pore} \mathbf{1}. \quad (75)$$

Constant pore pressure is assumed throughout the tissue, based on the assumption of connectedness of the pore space in the cell wall. Slight differences of swelling pressure across the cell wall because of varying chemical composition are not resolved here. The effect of the pore pressure at the macroscale is derived by the Biot tensor  $\mathbf{b}$  (cf. Eqs. (31), (35) and (38) for RVE-based, Eq. (15) for unit-cell-based, and Eq. (45) for laminate-based homogenization) at different length scales, connecting the isotropic pore pressure to anisotropic eigenstresses at the macroscopic scale. Macroscopic eigenstresses and eigenstrains are linked by (Zaoui 2002)

$$\Sigma_{SW_{ray}}^T = -\mathbb{C}_{SW_{ray}}^{hom, drained} : \mathbf{E}_{SW_{ray}}^T, \quad (76)$$

$$\text{where } \Sigma_{SW_{ray}}^T = -\mathbf{b}_{SW_{ray}}^{hom} \cdot p_{pore}^{sw}. \quad (77)$$

The macroscopic eigenstrains are linked to the tensor of linear hygroexpansion coefficients, related to the change of moisture content  $u$  as mass of water per mass of dry wood, through

$$\alpha_{SW_{ray}} = \frac{\partial \mathbf{E}_{SW_{ray}}^T}{\partial u}, \quad (78)$$

or, componentwise in the direction of the principal material directions of wood (no summation)

$$\alpha_{SW_{ray}, ii} = \frac{\partial E_{SW_{ray}, ii}^T}{\partial u}, \quad ii = [RR, TT, LL]. \quad (79)$$

In case of the small variations of the moisture content  $\Delta u = u_2 - u_1$  considered herein, the derivative may be approximated by a finite difference, reading as

$$\alpha_{SW_{ray}, ii} = \frac{E_{SW_{ray}, ii}^T(u_2) - E_{SW_{ray}, ii}^T(u_1)}{u_2 - u_1}, \quad ii = [RR, TT, LL]. \quad (80)$$

In a similar way, hygroexpansion coefficients can also be derived at smaller length scales by evaluating the eigenstrains at the respective scales. Also associated eigenstresses (free swelling at the macroscale does not necessarily mean stress-free conditions at all smaller length scales) can be determined that way.

The swelling pressure can be derived in the framework of thermodynamics, considering the different chemical potentials of the absorbed (bound) water and the water vapor in the environment, filling also partly the lumens. However, this goes beyond the scope of this paper, which focuses on the formulation of a multiscale model for the hygroelastic behavior of wood. Thus, in the following, the overall pore pressure  $p_{pore}^{sw}$  is back-calculated for particular moisture contents from macroscopic experimental data. A first check of the model is how the model represents swelling anisotropy, based on back-calculation of a scalar isotropic pore pressure. Thereon, the model is applied to study the hygroexpansion behavior across different length scales. Possible mechanosorptive effects at smaller length scales, which might occur during hygroexpansion, take effect on the back-calculated pore swelling pressure. Thus, these values might deviate from chemo-physical values following from differences in chemical potentials of the bound water and the free water in the lumens. In

summary, mechano-sorptive effects might spoil the purely physical character of the swelling pore pressure, however, they should not affect the suitability of the upscaling procedure.

## 6.2 Experimentally determined hygroexpansion coefficients - back-calculation of pore pressure

Macroscopic hygroexpansion coefficients of wood are usually determined by subjecting specimens with small dimensions in radial and tangential direction in a climate chamber to cycling relative humidity, for example between 30-90% as used by Bengtsson (2001). The measurements of the radial, tangential and longitudinal lengths are carried out inside the climate chamber. In addition the weight and the relative humidity are measured. After the cycles, the specimens are oven dried and weighed in order to determine the mass density in the dry state, serving as the basis for calculation of the moisture content at each measurement point. The eigenstrain in each direction between two moisture contents and, subsequently, the hygroexpansion coefficients are calculated from

$$u = \frac{m_u - m_0}{m_0} \cdot 100[\%], \quad (81)$$

$$\varepsilon_{ii} = \frac{L_{MC_1} - L_{MC_2}}{L_{MC_1}} \cdot 100[\%], \quad (82)$$

$$\alpha_{ii} = \frac{\varepsilon_{ii}}{u_{MC_1} - u_{MC_2}} [\%/ \%]. \quad (83)$$

For the hygroexpansion coefficients  $\alpha$  a behavior shown by (USDA 1999), with an increase of the radial and tangential coefficient up to 12% moisture content followed by a decrease to values of zero at high moisture contents, are considered herein. Mean values of the hygroexpansion coefficients are shown in Table 7.

For back-calculating the (isotropic) pore pressure from experimental results for hygroexpansion coefficients in the three principal material directions, the method of least squares is employed. For the mean hygroexpansion coefficients shown in Table 7 and typical microstructural characteristics of spruce wood as summarized in Section 2.1, the anisotropy of the hygroexpansion behavior is very well represented by the model, so that the resulting relative errors of the individual hygroexpansion coefficients are less than 1.2% in radial, 0.6% in tangential and 3.5% in longitudinal direction.

## 7. Application of the multiscale model

The multiscale model enables to investigate the effect of particular microstructural characteristics on the hygroexpansion behavior. In this context, the presented model is used to simulate the hygroexpansion at different wood densities (displayed as volume fractions of lumen) and varying moisture contents. Moreover, the model delivers insight into the hygroexpansion behavior at smaller length scales. It is applied in the following to predict hygroexpansion coefficients of the wood devices at different length scales, from the polymer network at microscale to softwood at macroscale, and to discuss contributions to the anisotropic hygroexpansion behavior.

Table 7 Mean values of hygroexpansion coefficients of spruce

$\alpha_T$	$\alpha_R$	$\alpha_L$	Reference
0.35	0.18	0.009	Bengtsson (2001)
0.35	0.19		Noack <i>et al.</i> (1973)
0.27 ... 0.36	0.15 ... 0.19		Wagenführ (2007)
0.33 ... 0.40	0.17 ... 0.22	0.00 ... 0.02	Persson (2000)
0.36	0.19	0.015	used in the model

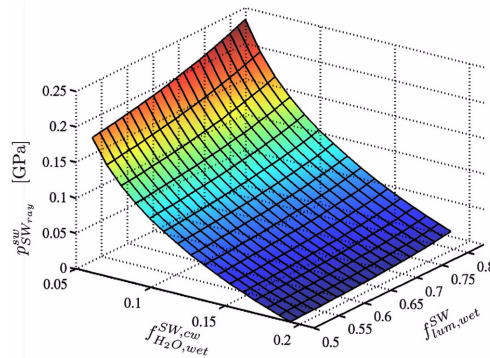


Fig. 13 Characteristics of the pressures in the pore space of softwood: swelling pore pressure  $p_{pore}^{sw}$  (colored surface) as function of the lumen volume fraction,  $f_{lum,swray}^{sw}$ , and of the cell wall-related volume fraction of water,  $f_{H_2O, wet}^{sw, cw}$ , typical for spruce

### 7.1 Influence of microstructural characteristics

Theoretical experiments have shown that the anisotropic hygroexpansion behavior is very sensitive to macroscopic and microscopic parameters, like the inclination angle of the radial cell wall or the densities of earlywood and latewood. The variation of the swelling pressure  $p_{pore}^{sw}$  with the cell-wall related volume fraction of water and the macroscopic volume fraction of lumens is shown in Fig. 13. Thereby, variable expansion coefficients with the moisture content, as described in Subsection 6.2, are used for determination of the swelling pressure.

The corresponding hygroexpansion coefficients, obtained with the back-calculated swelling pore pressure, are shown in Fig. 14. A detailed investigation of the influence of the microstructure on the macroscopic behavior was published in Gloimüller (2012).

### 7.2 Modeling of hygroexpansion at smaller length scales -an outlook

For the hygroexpansion behavior of wood hardly any experimental information can be found in literature, in particular for the expansion behavior of softwood at smaller length scales than the macroscopic one. The presented model provides a theoretical description of the hygroexpansion behavior of wood components at different length scales, therewith elucidating the origin of the anisotropic hygroexpansion behavior of wood. The expansion coefficients of polymer network in each cell wall layer, as the smallest investigated length scale, are shown in Table 8.

The consideration of water in form of spherical and ellipsoidal clusters elongated along the

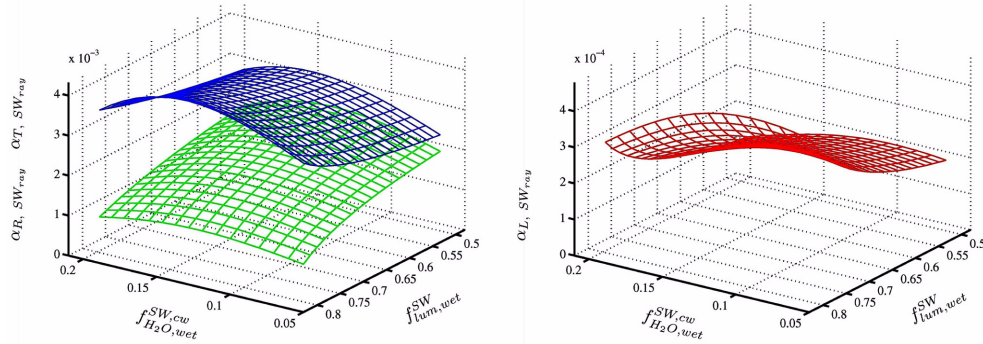


Fig. 14 Characteristics of the poromechanical model for softwood: Hygroexpansion coefficients in radial (lower lines), tangential (upper lines) and longitudinal direction (right lines) as functions of the lumen volume fraction,  $f_{lum,SW,cw}$ , and of the cell wall-related volume fraction of water,  $f_{H_2O,wet}^{SW,cw}$ , typical for spruce

Table 8 Microscale hygroexpansion coefficients for polymer network of the different cell wall layers in spruce. Direction  $L$  refers to the longitudinal direction of the ellipsoidally-shaped pores,  $T$  to the transversal direction with a transversal isotropic behavior. Since there are only negligible differences between the results for earlywood and latewood, only mean values are specified

	$ML$	$P$	$S1$	$S2$	$S3$
	poly	poly	poly	poly	poly
$\alpha_{TT}$ [%/%MC]	0.41	0.41	0.50	0.87	0.94
$\alpha_{LL}$ [%/%MC]	0.19	0.19	0.23	0.37	0.39
$\alpha_v$ [%/%MC]	1.02	1.02	1.23	2.13	2.30
$\alpha_{TT} / \alpha_{LL}$	2.13	2.13	2.18	2.34	2.40

microfibrils results in transversal isotropic expansion behavior of the polymer network throughout all cell wall layers. This constitutes the first contribution to anisotropic hygroexpansion of wood, with the smallest hygroexpansion in longitudinal direction, because of the cylindrical shape of the pores.

Table 9 shows hygroexpansion coefficients of each cell wall layer and of the entire cell wall, made up of the cell wall layers. Now,  $L$  refers to the macroscopic longitudinal material direction,  $R$  refers to the thickness direction of each cell wall layer, and  $T$  refers to the normal direction of the plane  $RL$ . The anisotropic hygroexpansion behavior of the cell wall layers causes from the interaction of the polymer network with the embedded microfibrils, inclined by the microfibril angle. Layer  $S1$  displays a high expansion in layer thickness direction because of the crossed alignment of the fibrils perpendicular to this direction. Together with layer  $S3$ , it restrains expansion in direction of the cell wall normal to the grain due to the high microfibril angles of these two layers. Layer  $S2$  shows a nearly transversal isotropic behavior and very low expansion in grain direction because of its low microfibril angle.

The anisotropic hygroexpansion behavior of the cell wall results from the interaction of the cell wall layers with different arrangements and inclinations of the microfibril. In longitudinal direction the cell wall hygroexpansion coefficient is very small because of the dominant behavior of the thick  $S2$  layer with a low microfibril angle. This effect is conserved up to the macroscopic scale where

Table 9 Multiscale hygroexpansion coefficients of spruce earlywood and latewood for the different cell wall layers and cell walls

MFA	Earlywood / Latewood					Cell wall
	<i>ML</i>	<i>P</i>	<i>S1</i>	<i>S2</i>	<i>S3</i>	
	<i>cwl</i>	<i>cwl</i>	<i>cwl</i>	<i>cwl</i>	<i>cwl</i>	
	75°	45°	50°	10/5°	75°	
$\alpha_{RR}$ [%/%MC]	0.40/0.40	0.40/0.40	0.53/0.51	0.48/0.48	0.59/0.59	0.54/0.51
$\alpha_{TT}$ [%/%MC]	0.08/0.08	0.21/0.21	0.10/0.11	0.47/0.48	0.05/0.05	0.27/0.37
$\alpha_{LL}$ [%/%MC]	0.38/0.38	0.21/0.21	0.08/0.08	0.03/0.02	0.55/0.55	0.031/0.025
$\alpha_v$ [%/%MC]	0.86/0.86	0.83/0.83	0.71/0.69	0.98/0.98	1.20/1.20	0.84/0.91
$\alpha_{RR} / \alpha_{TT}$	5.20/5.24	1.86/1.86	5.11/4.75	1.03/1.01	12.91/12.89	1.98/1.38
$\alpha_{TT} / \alpha_{LL}$	0.20/0.20	1.00/1.00	1.37/1.42	18.26/24.81	0.08/0.08	8.83/18.5
$\alpha_{RR} / \alpha_{LL}$	1.06/1.06	1.86/1.86	7.00/6.75	18.82/25.00	1.07/1.07	17.5/25.7

Table 10 Multiscale hygroexpansion coefficients of spruce earlywood (*EW*), latewood (*LW*) and softwood (*SW*) with and without restraining effect of rays

	Without rays			Restrained with rays		
	<i>EW</i>	<i>LW</i>	<i>SW</i>	<i>EW</i>	<i>LW</i>	<i>SW</i>
$\alpha_{RR}$ [%/%MC]	0.26	0.38	0.25	0.15	0.35	0.19
$\alpha_{TT}$ [%/%MC]	0.30	0.41	0.38	0.36	0.36	0.36
$\alpha_{LL}$ [%/%MC]	0.033	0.020	0.027	0.033	0.021	0.028
$\alpha_v$ [%/%MC]	0.59	0.82	0.66	0.55	0.73	0.58
$\alpha_{RR} / \alpha_{TT}$	0.87	0.92	0.66	0.43	0.96	0.53
$\alpha_{TT} / \alpha_{LL}$	9	21	14	11	17	13
$\alpha_{RR} / \alpha_{LL}$	8	19	9	5	17	7

wood shows the smallest expansion coefficients also in longitudinal direction. The highest hygroexpansion of the cell wall is observed in its thickness direction, because no microfibrils are oriented in this direction. Comparing the hygroexpansion coefficients of the cell wall in *R* and in *T* direction, respectively, shows a mean expansion in cell wall thickness direction. Overlaying the shapes of a unit cell lumen before and after hygroexpansion combined with the small expansion of the cell walls in its direction, confirms that the volume of the lumen only changes slightly during hygroexpansion, as documented before by several researchers (Derome *et al.* 2011, Kollmann 1951).

Table 10 shows hygroexpansion coefficients of earlywood and latewood as well as their interaction in softwood, evaluating also the restraining effect of ray cells in the radial direction.

The final output of the model - the macroscopic hygroexpansion coefficients, shown in Table 10, describe well the hygroexpansion behavior of spruce softwood in qualitative and quantitative terms. The largest contribution to the anisotropic expansion behavior of wood arises from the interaction of earlywood and latewood. Latewood shows a nearly transversal isotropic expansion behavior. In earlywood and latewood, the cell walls run continuously from pith to the bark in radial direction, while they are staggered in tangential direction. Thus, the high expansion in the thickness direction (cf.  $\alpha_{RR}$  of the cell wall from Table 9) can take full effect in tangential direction. The discontinuity of the tangential walls restrain the radial expansion resulting from the layers with high microfibril

angles arranged in radial direction at the cell corners. Because of its high volume fraction earlywood controls the anisotropic hygroexpansion behavior of softwood. Ray cells reduce the expansion in radial direction due to their alignment in this direction, further increasing the ratio between hygroexpansion in radial and tangential direction.

## 8. Conclusions

We herein studied the microstructural origin of the anisotropy and the macroscopic hygroexpansion behavior of wood in a quantitative framework. By applying poromechanics, we could link a microscale swelling pressure in the amorphous polymer matrix of the wood cell wall to macroscale dimensional changes. Therewith, the individual contributions of structural features at various length scales, such as different swelling behaviors of the cell wall layers, induced by varying microfibril angles, cell wall layer thicknesses and chemical compositions, the restraining effect of ray cell bundles, or the interaction of earlywood and latewood, to the macroscopic behavior could be investigated. The microporomechanical model comprises six homogenization steps at five levels, which are performed by means of continuum (poro) micromechanics, the unit cell method and the laminate theory. As for the latter two, also poromechanical formulations were employed.

Restraining of earlywood and latewood by ray cell bundles and their interaction at the macroscopic scale were found to show a pronounced effect on the anisotropic hygroexpansion behavior. At the microscopic scale, the microfibril angles of the different cell wall layers are very relevant. In particular, the circumferential orientation of the fibers in the S3 layer and the resulting restraining of a wood cell affects the macroscopic hygroexpansion behavior. The presented model is applicable at moisture contents of 5 to 20%. The suitability of the model is underlined by the good agreement of predicted stiffnesses with corresponding experimental results across this moisture content range. This moisture content range includes the changes generally observed at wood constructions, so that the presented model constitutes a valuable tool for practical considerations on wood hygroexpansion in timber engineering.

## Acknowledgements

The authors gratefully acknowledge the financial support of the Austrian Research Promotion Agency (FFG, project number 815234/12791) and the wood industry partnership “Building with Wood” within CEI-Bois for funding the research work within project “MechWood”. This work forms part of that project.

## References

- Astley, R., Stol, K. and Harrington, J.J. (1998), “Modelling the elastic properties of softwood, part ii: The cellular microstructure”, *Holz Roh Werkst.*, **56**(1), 43-50.
- Bader, T.K., Hofstetter, K. and Eberhardsteiner, J. (2011), “The poroelastic role of water in cell walls of the hierarchical composite “softwood”, *Acta Mech.*, **217**(1-2), 75-100.

- Bengtsson, C. (2001), "Variation of moisture induced movements in norway spruce (*picea abies*)", *Ann. Forest Sci.*, **58**(5), 569-581.
- Bergander, A. (2001), *Local variability in chemical and physical properties of spruce wood fibers*, Doctoral thesis, Royal Institute of Technology.
- Biot, M.A. (1955), "Theory of elasticity and consolidation for a porous anisotropic solid", *J. Appl. Phys.*, **26**(2), 182-185.
- Böhm, H. (2004), *A short introduction to continuum micromechanics*, Springer Verlag, Wien, New York.
- Boutelje, J.B. (1962), "The relationship of structure to transverse anisotropy in wood with reference to shrinkage and elasticity", *Holzforschung*, **16**(2), 33-46.
- Burgert, I. (2000), *Die mechanische bedeutung der holzstrahlen im lebenden baum*, Doctoral thesis, University Hamburg.
- Burgert, I. (2003), "Über die mechanische bedeutung der holzstrahlen", *Schweiz. Z. Forstwes.*, **154**(12), 498-503.
- Derome, D., Griffa, M., Koebel, M. and Carmeliet, J. (2011), "Hysteretic swelling of wood at cellular scale probed by phase-contrast x-ray tomography", *J. Struct. Biol.*, **173**(1), 180-190.
- Dormieux, L., Molinari, A. and Kondo, D. (2002), "Micromechanical approach to the behavior of poroelastic material", *J. Mech. Phys. Solids*, **50**(10), 2203-2231.
- Eitelberger, J. and Hofstetter, K. (2011), "Prediction of transport properties of wood below the fiber saturation point -a multiscale homogenization approach and its experimental validation, part I: Thermal conductivity", *Compos. Sci. Technol.*, **71**(2), 134-144.
- El Omri, A., Fennan, A., Sidorov, F. and Hihi, A. (2000), "Elastic-plastic homogenization for layered composites", *Eur. J. Mech. A-Solid*, **19**(4), 585-601.
- Elwood, E. (1954), *Properties of american beech in tension and compression perpendicular to the grain and their relation to drying*, Yale Univ. School For., Bull. No. 61, Yale Univ., New Haven, CT.
- Farruggia, F. and Perré, P. (2000), "Microscopic tensile tests in the transverse plane of earlywood and latewood parts of spruce", *Wood Sci. Technol.*, **34**(2), 65-82.
- Fengel, D. and Wegener, G. (1983), *WOOD Chemistry, Ultrastructure, Reactions*, Verlag Kessel, Munich.
- Fratzl, P. and Weinkamer, R. (2007), "Nature's hierarchical material", *Prog. Mater. Sci.*, **52**(8), 1263-1334.
- Gloimüller, S. (2012), *Multiscale modeling and experimental investigation of the hygroexpansion behavior of softwood*, Doctoral thesis, Vienna University of Technology, Faculty of Civil Engineering. In English.
- Greenhill, W. (1936), "Strength tests perpendicular to the grain of timber at various temperatures and moisture contents", *J. Counc. Sci. Ind. Res.*, **9**(4), 265-278.
- Hellmich, C. and Ulm, F.J. (2005), "Drained and undrained poroelastic properties of healthy and pathological bone: A poro-micromechanical investigation", *Transport Porous Med.*, **58**(3), 243-268.
- Hofstetter, K., Hellmich, C. and Eberhardsteiner, J. (2006), "Micromechanical modeling of solid-type and plate-type deformation patterns within softwood materials. A review and an improved approach", *Holzforschung*, **61**(4), 343-351.
- Kadita, S., Yamada, T., Suzuki, M. and K., K. (1961), "Studies on the rheological properties of wood. i. effect of moisture content on the dynamic young's modulus of wood. ii. effect of heat-treating condition on the hygroscopicity and dynamic young's modulus of wood", *J. Jap. Wood Res. Soc.*, **7**(1), 29-38.
- Kifetew, G. (1997), "Application of the earlywood-latewood interaction theory to the shrinkage anisotropy of scots pine", *International Conference of COST Action E8, Mechanical Performance of Wood and Wood Products, Theme: Wood-water relations*, Royal Institute of Technology Stockholm, Sweden.
- Kifetew, G., Lindberg, H. and Wiklung, M. (1997), "Tangential and radial deformation field measurements on wood during drying", *Wood Sci. Technol.*, **31**(1), 35-44.
- Kollmann, F. (1951), *Technologie des holzes und der holzwerkstoffe*, Verlag Springer, Berlin, Heidelberg, New York.
- Kufner, M. (1978), "Modulus of elasticity and tensile strength of wood species with different density and their dependence on moisture content", *Holz Roh. Werkst.*, **36**(11), 435-439.
- Lindström, H. (1996), "Fiber length, tracheid diameter, and latewood percentage in norway spruce: Development from pith outwards", *Wood Fiber Sci.*, **29**(1), 21-34.
- Marklund, E. and Varna, J. (2009), "Modeling the hygroexpansion of aligned wood fiber composites", *Compos. Sci. Technol.*, **69**(7-8), 1108-1114.

- Moden, C.S. and Berglund, L.A. (2008a), "Elastic deformation mechanisms of softwoods in radial tension -cell wall bending or stretching?", *Holzforschung*, **62**(5), 562-568.
- Moden, C.S. and Berglund, L.A. (2008b), "A two-phase annual ring model of transverse anisotropy in softwoods", *Compos. Sci. Technol.*, **68**(14), 3020-3026.
- Nakano, T. (2008), "Analysis of cell wall swelling on the basis of a cylindrical model", *Holzforschung*, **62**(3), 352-356.
- Neagu, R. and Gamstedt, E. (2007), "Modelling of effects of ultrastructural morphology on the hygroelastic properties of wood fibres", *J. Mater. Sci.*, **42**(24), 10254-10274.
- Neuhaus, T.H. (1981), *Elastizitätszahlen von fichtenholz in abhängigkeit von der holzfeuchte*, Technisch-wissenschaftliche Mitteilungen 81-8, Institut für Konstruktiven Ingenieurbau, Ruhr-Universität Bochum.
- Noack, D., Schwab, E. and Bartz, A. (1973), "Characteristics for a judgment of the sorption and swelling behavior of wood", *Wood Sci. Technol.*, **7**(3), 218-236.
- Olsson, T., Megnis, M., Varna, J. and Lindberg, H. (2001), "Study of the transverse liquid flow paths in pine and spruce using scanning electron microscopy", *J. Wood Sci.*, **47**(4), 282-288.
- Pang, S. (2002), "Predicting anisotropic shrinkage of softwood part 1: Theories", *Wood Sci. Technol.*, **36**(1), 75-91.
- Pang, S. and Herritsch, A. (2005), "Physical properties of earlywood and latewood of *pinus radiata* d. don: Anisotropic shrinkage, equilibrium moisture content and fibre saturation point", *Holzforschung*, **59**, 654-661.
- Perré, P. and Huber, F. (2007), "Measurement of free shrinkage at the tissue level using an optical microscope with an immersion objective: results obtained for douglas fir (*pseudotsuga menziesii*) and spruce (*picea abies*)", *Ann. Forest Sci.*, **64**(3), 255-265.
- Persson, K. (2000), *Micromechanical modelling of wood and fibre properties*, Doctoral thesis, Lund University. In English.
- Qing, H. and Mishnaevsky Jr., L. (2008), *3d hierarchical computational model of wood as a cellular material with bril reinforced, heterogeneous multiple layers*, Mechanics of Materials.
- Qing, H. and Mishnaevsky Jr., L. (2009), *Moisture-related mechanical properties of softwood: 3d micromechanical modeling*, Computational Materials Science.
- Schneider, A. (1971), "Investigations on the influence of heat treatments with a range of temperatures from 100° to 200°C on the modulus of elasticity, maximum crushing strength, and impact work of pine sapwood and beechwood", *Holz Roh. Werkst.*, **29**(11), 431-440.
- Siimes, F. (1967), "The effect of specific gravity, moisture content, temperature and heating time on the tension and compression strength and elastic properties perpendicular to the grain of Finnish pine, spruce and birch wood and the significance of those factors on the checking of timber at kiln drying", *State Inst. Tech. Res., Helsinki, Finland*, 84.
- Smith, S.A. and Langrish, T.A.G. (2008), "Multicomponent solid modeling of continuous and intermittent drying of *pinus radiata* sapwood below the fiber saturation point", *Dry. Technol.*, **26**(7), 844-854.
- Sulzberger, P. (1953), *The effect of temperature on the strength of wood, plywood and glue joints*, Aeronaut. Res. Consultative Com. Rep. ACA-46, Melbourne, Australia.
- Tarmian, A. and Azadfallah, M. (2009), "Variation of cell features and chemical composition in spruce consisting of opposite, normal, and compression wood", *BioResource.*, **4**(1), 194-204.
- Ulm, F.J., Delafargue, A. and Constantinides, G. (2004), "Experimental microporomechanics", *Lecture notes prepared for the summer school Applied Micromechanics of Porous Materials, Coordinated by L. Dormieux and F.-J. Ulm*, International Centre for Mechanical Sciences (CISM), Udine, Italy.
- USDA (1999), *Wood handbook*, U.S. Department of Agriculture, United States of America.
- Wagenführ, R. (2007), *Holzatlas*, Fachbuchverlag Leipzig im Carl Hanser Verlag, Leipzig, 6. edition.
- Watanabe, U., Fujita, M. and Norimoto, M. (2002), "Transverse young's moduli and cell shapes in coniferous early wood", *Holzforschung*, **56**(1), 1-6.
- Wilson, R. (1932), *Strength-moisture relations of wood*, USDA Tech. Bull. No. 282 U.S. Dep. Agric., Washington, D.C.
- Yamamoto, H. (1999), "A model of the anisotropic swelling and shrinking process of wood. Part 1: Generalization of Barber's wood fiber model", *Wood Sci. Technol.*, **33**(4), 311-325.
- Zaoui, A. (2002), "Continuum micromechanics: Survey", *J. Eng. Mech.*, **128**(8), 808-816.

**Nomenclature:** *length scales of softwood*

SW ... softwood  
 AR ... annual ring  
 EW ... earlywood  
 LW ... latewood  
 ray ... ray cell bundles  
 cw ... cell wall  
 cwl ... cell wall layer  
 ML ... middle lamella  
 P ... primary wall  
 S<sub>1</sub>-S<sub>3</sub> ... first up to third secondary wall

**Nomenclature:** *chemical composition of softwood*

CC ... crystalline cellulose  
 AC ... amorphous cellulose  
 C ... cellulose, sum of crystalline and amorphous fractions  
 HC ... hemicellulose  
 L ... lignin  
 EXT ... extractives  
 H<sub>2</sub>O ... water  
 chem ... chemical components (without H<sub>2</sub>O)  
 $\rho$  ... density of: chemical components  $\rho_{chem}$ , cell wall layers  $\rho_{cwl}$ , cell wall  $\rho_{cw}$ , annual rings  $\rho_{EW/LW}$  and softwood  $\rho_{SW}$

**Nomenclature:** *fractions and moisture*

$f$  ... volume fraction  
 $wf$  ... weight fraction  
 dry ... dry condition  
 wet ... wet condition  
 MC ... moisture content of wood  
 RH ... relative humidity of the ambient air  
 sc ... sorption capacity at all length scales  
 sw ... swelling

**Nomenclature:** *homogenization techniques*

UC ... unit cell method  
 MT ... Mori Tanaka scheme  
 SC ... self consistent scheme  
 LT ... laminate theory  
 $\mathbb{C}, \mathbb{c}$  ... fourth-order stiffness tensor  
 $\mathbb{A}$  ... fourth-order strain concentration tensor  
 $\mathbb{B}$  ... fourth-order stress concentration tensor  
 $\mathbb{P}$  ... fourth-order Hill tensor  
 $\mathbb{I}$  ... fourth-order unity tensor  
 $S$  ... sorting matrix operator

$\mathbf{b}$  ... second-order Biot tensor  
 $\mathbf{E}, \boldsymbol{\varepsilon}$  ... second-order strain tensor (macro and microscale)  
 $\boldsymbol{\alpha}$  ... second-order hygroexpansion tensor  
 $\boldsymbol{\Sigma}, \boldsymbol{\sigma}$  ... second-order stress tensor (macro and microscale)  
 $N$  ... first-order Biot modulus  
 $M$  ... first-order overall Biot modulus  
 $k$  ... first-order bulk modulus  
 $p, \Pi$  ... pore pressure  
 $hom$  ... homogenized

**Nomenclature:** *geometrical dimensions*

$R, T$  and  $L$  ... macroscopic radial, tangential and longitudinal direction  
 $\varphi$  ... inclination angle between radial and tangential cell wall  
 $\beta$  ... widening angle between axis and surface of a cell wall  
 $\ell_R, \ell_T$  ... radial and tangential dimensions of a wood cell  
 $\theta$  ... microfibril angle (MFA)  
 $\phi$  ... porosity,  $f_{pores}$

Indices after a comma refer to tensor components and not to partial differentiation.